

Response to Associate Editor Comments  
(G. Gehrels, 10 July, 2020)

Blue = AE comments from 26 March 2020

Green = AE comments from 17 June 2020

Black = author response to comments

Red = changes to manuscript

Responses to the AE comments are inserted below.

**Sharman Review:**

1. Dr. Sharman gave a positive review that raises one major point and several minor ones. The major concern was about the lack of evidence to support the inference that near depositional age zircon is air-fall in origin and older zircon is recycled. You responded to this comment by saying that you are:

unable to provide reliable information about morphology of the young grains, as most were plucked out from the mounts and dissolved for CA-TIMS geochronology. We tried to do this analysis with BSE images of the grains (before analysis), but the size/shape of the grains in the images has little bearing on the true size/shape of the grains. This because the mounts were polished down just a little so as to retain more material for the CA-TIMS analyses.

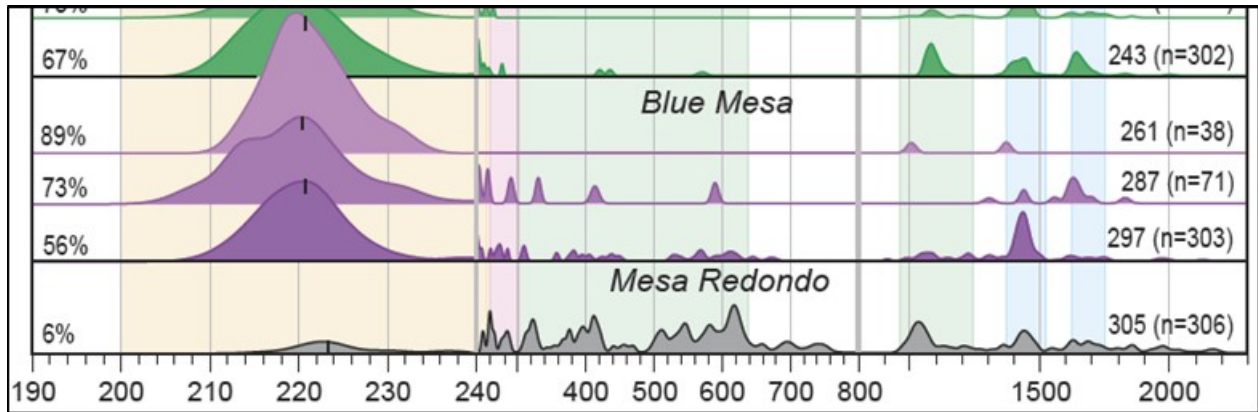
I would have thought that even a two-dimensional cross section through a c-axis parallel zircon grain would reveal whether the grain is prismatic or not. If you have stored the BSE images, then I would encourage you to include them in an online data repository.

Response: We would love to be able to provide this info, as it would be great test of our interpretations concerning air-fall versus detrital zircons. Unfortunately, we just can't extract reliable information from the BSE images because the mounts were polished down just far enough to expose a little bit of each crystal. It's just not possible to say anything reliable about grain shape from the BSE images. We also are unable to go back and look at the grains in the mounts as many have been removed from the mount for CA-TIMS analysis.

2. The reviewer also has a question about the change in scale of your age distributions. An alternative way to bump the height of the pre-240Ma age component would be to plot the age distributions on a logarithmic time scale. Furthermore, if you replace your Probability Density Plots (PDPs) by Kernel Density Estimates (KDEs), then you can tweak their bandwidth to produce the most informative result. As you know, cumulative distributions are also useful for data visualization. They, too, can be plotted on a logarithmic time axis.

PDP vs KDE: I won't fight with you over this. If you want to use PDPs to visualise your data then that is fine with me. But please don't use them for quantitative analysis.

Response: Indeed, there are several different options for showing the age distributions, and we have experimented with a few. In our view, none of the other options (e.g., log scale or cumulative plots) show the details of the Triassic ages, and the proportions and ages of the older components, as clearly as the current plot (a portion of which is shown below).



Response: Ages distributions remain as PDP's, quantitative analyses are now conducted with KDE's.

#### Ramezani Review:

1. Stratigraphy: Dr Ramenazi is concerned that the observed drift between your MDAs and the depositional ages is due to misidentification of the stratigraphic positions in the CPCP core. In your response, you wrote that your paper does not aim to present an age model, and does not claim to estimate accurate MDAs either. I am a bit confused, because the paper does seem to me like an attempt to calibrate the depositional history of the CPCP core in absolute time. If your paper has a different objective, then please state more clearly what the purpose of the study actually is. I apologise if I am missing something obvious here.

Age models: I won't fight over this either. I understand that you don't present a new age model. But what then is the purpose of the MDA estimates?

Correct, LA-ICPMS data are not used to construct an age model. The age model shown is based on magnetostratigraphy (Kent et al., 2019), with constraints from CA-TIMS (Rasmussen et al., 2020).

The purpose of the MDA's is to provide an estimate of the age of the main cluster of dates from each sample. Comparison of these MDA's with the age model yields two conclusions of geological significance:

First, MDA's overlap with the age model for fine-grained strata but are a few m.y. older for coarse-grained strata. This is interpreted to record the presence of mainly air-fall (depo-age) zircons in the fine-grained strata, whereas coarser-grained strata are dominated by older/recycled grains.

Second, MDA's for sandstones are similar for tens of meters of stratigraphy, whereas the age model youngs upward (of course). This provides interesting information about patterns of recycling of older grains in the Chinle fluvial system.

2. U-Pb geochronology: Dr. Ramenazi is concerned that the LA-ICP-MS results may be affected by Pb-loss, which would invalidate their use as maximum depositional ages. In your response, you write that:

This manuscript goes to great length to document that Pb loss is a significant factor for many of the grains analyzed. We show this internally with the Uconc-age tests described above. We also document this by comparison of our ages with the CA-TIMS data from the same grains (Appendix 2). Indeed, Pb loss is an important factor for many of our analyses! But the assertion that LA-ICPMS max depo ages are younger than the CA-TIMS ages of Ramezani et al. (2011) and Atchley et al. (2013) due to Pb loss is not supported by the fact that most of the reported LA-ICPMS MDA's are older (not younger) than the equivalent MDA's reported by R+2011 and A+ 2013!!

Appendix 2 clearly shows that the LA-ICP-MS data are consistently 5-10 Ma younger than the CA-TIMS ages. To me this confirms the reviewer's concerns. The fact that the ad-hoc MDA estimates for the youngest LA-ICP-MS peak (which are shown as circles in Appendix 2) are consistently older than the CA-TIMS estimates (which are shown as red bars in Appendix 2) is a result of comparing datasets of different size. Your LA-ICP-MS based MDA estimate uses more grains than the CA-TIMS estimate, making the comparison between the two estimates biased. This problem is diagnostic of a fundamental flaw in three of the four MDA estimation algorithms that are proposed in the manuscript. I will discuss this in more detail below.

Maximum depositional ages: it would be great if you could give the Galbraith approach a try. If you like it then that would solve this issue.

I have used the RadialPlotter routine in IsoplotR to calculate Minimum Ages for all samples. The results are reported in Table 6, shown on Figures 5 and 13 and Appendix 2, and discussed in the revised text. These are interpreted to represent the most reliable Max Depo Age for each sample.

The manuscript has been revised to present minimum ages for all samples, and to explore the implications of the patterns of these ages for the present data set and for the utility of the minimum age model.

## Further Comments:

1. The paper uses four different heuristic MDA estimation algorithms. Three of these methods are problematic, because they drift to ever younger ages with increasing sample size.

(a) Age of the youngest peak on a probability density plot (PDP): PDPs have no statistical basis, and any quantitative information derived from them is of dubious statistical significance. If you were to analyse one million grains of zircon, then the youngest age cluster on a PDP would likely be younger than the actual depositional age.

(b) Weighted Mean age and uncertainty of the youngest cluster: Same problem. Any heuristic method that is based on p-values is problematic because p-values are a sensitive function of sample size. The larger the sample size, the greater the likelihood that the  $\chi^2$ -test identifies spurious peaks.

(c) Maximum Likelihood age and uncertainty. See Figure 6.3 of Vermeesch (2018b) for an example of how multimodal unmixing models suffer from the same problem as methods a. and b.

The sample size dependency is actually reported in the paper (“Ironically, the more grains analyzed, the greater the inaccuracy of [the] youngest age!”). I do not understand why these broken methods are still used in the paper and would advocate that they are removed. In statistics, it is desirable for estimates to asymptotically converge to the truth with increasing sample size. Only the Tuffzirc age model may have this property. An alternative would be the parametric minimum age model of Galbraith and Laslett (1993). But neither of these techniques is immune to the Pb-loss problem.

Maximum depositional ages: it would be great if you could give the Galbraith approach a try. If you like it then that would solve this issue.

We have addressed these comments in two ways:

1. To represent the AE's concerns about the statistical validity of these methods, we have noted in the Analytical Methods section that Vermeesch (2018b) has documented issues with the robustness of all of these methods.

2. As noted above, we have applied the minimum age model, and it provides a more reliable MDA for most samples.

The revised text explores all of these issues, and concludes with a discussion of the power of the minimum age method for addressing both simple and complex age distributions.

2. The paper frequently uses two ad-hoc dissimilarity measures called ‘Likeness’ and ‘Cross-correlation Coefficient’ (CCC). These quantities are both derived from PDPs and are flawed for

reasons that are given in detail by Vermeesch (2018a). Please remove these from the paper and replace them with bona fide statistical dissimilarity measures such as the Kolmogorov-Smirnov statistic. Of course, if you can present a statistically valid argument against my objections to Likeness and CCC, then I would be happy to change my mind.

Likeness and cross correlation: here I am going to stand my ground.

Done -- Likeness, Similarity, and Cross Correlation these have been removed!

Statistical comparisons using Likeness, Similarity, and Cross Correlation have been removed. All discussion of these methods has been removed. DR Tables 4 and 5 now report comparisons using KS-D values and Kuiper-V values.

MDS plots (Figures 9 and 11) have been remade using KS-D values.

3. Is Figure 10 a two-dimensional PDP or KDE? I think that this diagram would be more effective as a contour plot, or as a simple scatter plot. The three-dimensional effect adds no useful information.

Response: These are based on two-dimensional KDE's. With regard to the 3-d effect, I think this helps readers evaluate similarities/differences of the various units.



23 **ABSTRACT**

24 U-Pb geochronology was conducted by Laser Ablation-Inductively Coupled Plasma Mass  
25 Spectrometry (LA-ICPMS) on [7,175](#) detrital zircon grains from twenty-nine samples from the  
26 Coconino Sandstone, Moenkopi Formation, and Chinle Formation. These samples were  
27 recovered from ~520 m of drill core that was acquired during the Colorado Plateau Coring  
28 Project (CPCP), located in Petrified Forest National Park (Arizona).

29 A sample from the lower Permian Coconino Sandstone yields a broad distribution of  
30 Proterozoic and Paleozoic ages that are consistent with derivation from the Appalachian and  
31 Ouachita orogens, with little input from local basement or Ancestral Rocky Mountain sources.  
32 Four samples from the Holbrook Member of the Moenkopi Formation yield a different set of  
33 Precambrian and Paleozoic age groups, indicating derivation from the Ouachita orogen, the  
34 East Mexico Arc, and the Permo-Triassic arc built along the Cordilleran margin.

35 Twenty-three samples from the Chinle Formation contain variable proportions of Proterozoic  
36 and Paleozoic zircon grains, but are dominated by Late Triassic grains. LA-ICPMS ages of these  
37 grains belong to five main groups that correspond to the Mesa Redondo Member, Blue Mesa  
38 Member and lower part of the Sonsela Member, upper part of the Sonsela Member, middle  
39 part of the Petrified Forest Member, and upper part of the Petrified Forest Member. The ages  
40 of pre-Triassic grains also correspond to these chronostratigraphic units, and are interpreted to  
41 reflect varying contributions from the Appalachian orogen to the east, Ouachita orogen to the  
42 southeast, Precambrian basement exposed in the Ancestral Mogollon Highlands to the south,  
43 East Mexico arc, and Permian-Triassic arc built along the southern Cordilleran margin. Triassic  
44 grains in each chronostratigraphic unit also have distinct U and Th concentrations, which are  
45 interpreted to reflect temporal changes in the chemistry of arc magmatism.

46 Comparison of our LA-ICPMS ages with available CA-TIMS ages and new magnetostratigraphic  
47 data provides new insights into the depositional history of the Chinle Formation, as well as  
48 methods utilized to determine depositional ages of fluvial strata. For parts of the Chinle  
49 Formation that are dominated by fine-grained clastic strata (e.g. mudstone and siltstone), such  
50 as the Blue Mesa Member and Petrified Forest Member, all three chronometers agree (to  
51 within ~1 m.y.), and robust depositional chronologies have been determined. In contrast, for  
52 stratigraphic intervals dominated by coarse-grained clastic strata (e.g., sandstone), such as  
53 most of the Sonsela Member, the three chronologic records disagree due to recycling of older  
54 zircon grains and variable dilution of syn-depositional-age grains. This results in LA-ICPMS ages  
55 that significantly pre-date deposition, and CA-TIMS ages that range between the other two  
56 chronometers. These complications challenge attempts to establish a well-defined  
57 chronostratigraphic age model for the Chinle Formation, ~~and to evaluate possible connections~~  
58 ~~among fundamental Late Triassic biotic and climatic changes and a red siliceous horizon~~  
59 ~~encountered in the CPCP core.~~

## 60 1. INTRODUCTION

61 Triassic strata of the Colorado Plateau and environs provide rich and geographically extensive  
62 records of environmental and biotic change during a critical period of Earth history, as well as  
63 the transition from passive- to convergent-margin tectonism along the North American  
64 Cordillera (e.g., Parker and Martz, 2011; Olsen et al., 2011). As demonstrated by Riggs et al.  
65 (1996, 2003, 2012, 2013, 2016), Dickinson and Gehrels (2008), Irmis et al. (2011), Ramezani et  
66 al. (2011, 2014), Atchley et al. (2013), Nordt et al. (2015), Kent et al. (2018, 2019), Olsen et al.  
67 (2018, 2019), Marsh et al. (2019), and Rasmussen et al. (202019), Chinle Formation strata have  
68 the potential to record the timing of these changes in great detail given their several-hundred-  
69 meter thickness, abundance of near-depositional-age zircon grains, and recoverable  
70 paleomagnetic reversal stratigraphy.

71 In an effort to further develop this record, ~520 m of continuous core was collected from  
72 Triassic and underlying Permian strata at Petrified Forest National Park (PEFO), which is located  
73 on the southern Colorado Plateau of northern Arizona (Fig. 1; [\(35.085933° N, 109.795500° W,](#)  
74 [WGS84 datum\)](#)). The objectives and primary findings of this project have been described by  
75 Olsen et al. (2018, 2019), Kent et al. (2018, 2019), and Rasmussen et al. (202019), and  
76 numerous related studies are currently in progress. This contribution to the project reports ~~on~~  
77 U-Pb geochronologic analyses of detrital zircon grains that were extracted from twenty-nine  
78 samples from this core (CPCP-PFNP13-1A). Analyses were conducted by laser ablation-  
79 inductively coupled mass spectrometry (LA-ICPMS), with between 36 and 490 grains analyzed  
80 per sample ([total of 7,175 analyses](#)). Grains were chosen for analysis by random selection in an  
81 effort to provide unbiased information about provenance. Fortunately, a significant number of  
82 near-depositional-age grains were recovered from many samples in the Chinle Formation,  
83 which provides opportunities to also determine robust maximum depositional ages. This report  
84 explores variations in both provenance and maximum depositional age of strata intersected in  
85 the CPCP-PFNP13-1A core, and the implications for Permian-Triassic environmental and biotic  
86 transformations and the tectonic evolution of southwestern North America.

## 87 2. STRATA ENCOUNTERED IN THE PETRIFIED FOREST NATIONAL PARK DRILL CORE

88 The lowest stratigraphic horizon encountered consists of quartz arenite belonging to the  
89 Coconino Sandstone (Fig. 2). This unit belongs to regionally extensive erg deposits of early  
90 Permian (Leonardian) age (Blakey et al., 1988; Lawton et al., 2015; Dickinson, 2018).

91 Overlying strata of the Coconino Sandstone are tabular, thin to thick-bedded, reddish  
92 mudstone, siltstone, and sandstone layers of the Lower-Middle Triassic Moenkopi Formation. In  
93 the PEFO region, the Moenkopi Formation consists of thin-bedded reddish siltstone with  
94 interlayered sandstone and mudstone. Lower, finer-grained strata are assigned to the Wupatki  
95 Member and Moqui Member, and upper sandstone-rich horizons dominate the Holbrook  
96 Member. The base is a regional unconformity, the TR-1 unconformity of Pipiringos and  
97 O'Sullivan (1978), along which strata of the lower Permian Toroweap Formation and Kaibab



98 Formation have been removed. Strata of the Moenkopi Formation are interpreted to have  
99 accumulated on a northwest-sloping coastal plain, with thinner fluvial strata to the southeast  
100 and thicker marginal marine strata to the northwest (Dickinson, 2018). The Moenkopi  
101 Formation basin was bounded by residual uplifts of the Ancestral Rocky Mountains to the  
102 northeast and highlands of the Ouachita orogen to the southeast. Highlands developed within  
103 early phases of the Cordilleran magmatic arc may have existed to the southwest.

104 Strata of the Moenkopi Formation are overlain unconformably [Tr-3 unconformity of Pippingos  
105 and O'Sullivan (1978)] by the Chinle Formation (Fig. 2). The transition is marked in most areas  
106 by the Shinarump Conglomerate, which consists of cobbles of chert, quartzite, limestone and  
107 subordinate felsic volcanic rocks. Riggs et al. (2012) have determined U-Pb ages of 232-224 Ma  
108 on volcanic cobbles in the Shinarump Conglomerate. The Shinarump Conglomerate is  
109 interpreted to correlate with finer-grained strata of the Mesa Redondo Member (Irmis et al.,  
110 2011; Martz et al., 2012, 2017; Riggs et al., 2016). Strata of the Shinarump Conglomerate and  
111 Mesa Redondo Member are interpreted to have accumulated in paleovalleys that were carved  
112 into underlying strata. Strikingly variegated, strongly pedogenically modified, red, purple, and  
113 yellow strata in the core are assigned to the Mesa Redondo Member given the lack of  
114 conglomerate. Strata of the Mesa Redondo Member in outcrop have yielded U-Pb (~~U-Pb~~ zircon)  
115 ages of ~227.6 Ma (Atchley et al., 2013) and ~225.2 Ma (Ramezani et al., 2011).

116 Gradationally overlying the Mesa Redondo Member are strata of the Blue Mesa Member,  
117 which consist of purplish to gray and red bentonitic mudstone with sandstone beds that are  
118 generally 0.5 m in thickness (Woody, 2006). Blue Mesa Member mudstones are pervasively  
119 pedogenically modified in the core. These strata are interpreted to have accumulated primarily  
120 as overbank deposits within a mixed-load meandering river system (Martz and Parker, 2010).  
121 Previously reported U-Pb (ID-TIMS or CA-TIMS) ages from outcrop of the Blue Mesa Member  
122 range from ~223 Ma to ~218 Ma (Heckert et al., 2009; Ramezani et al., 2011; Irmis et al., 2011;  
123 Atchley et al., 2013; Rasmussen et al., ~~2014~~2019).

124 Strata of the Blue Mesa Member are overlain by sandstone-rich and conglomerate-bearing  
125 strata of the Sonsela Member. Lucas (1993) and Heckert and Lucas (2002) refer to the base of  
126 the Sonsela Member as a regionally significant unconformity, although this interpretation has  
127 been questioned by Woody (2006) and Martz and Parker (2010) given that conglomeratic  
128 sandstone of the Sonsela is interbedded with mudstone of the Blue Mesa Member. Martz and  
129 Parker (2010) suggest that the transition from the Blue Mesa Member to the Sonsela Member  
130 marks a change in depositional regime (from mainly overbank deposits to bedload-dominated  
131 channel deposits) but does not mark a significant hiatus in deposition.

132 The Sonsela Member consists predominantly of sandstone with lesser mudstone and local  
133 conglomerate. Sandstone beds are variable in thickness, have significant lateral extent, and  
134 exhibit cut-and-fill structure (Woody, 2006). Conglomerate (with abundant volcanic clasts) is  
135 common within the sandstone beds. Five units have been recognized, a lower sandstone  
136 interval (Camp Butte beds), a lower-middle unit with abundant mudstone (Lot's Wife beds), a

137 middle sandstone and conglomerate unit (Jasper Forest/Rainbow Forest bed), a middle-upper  
138 unit with pedogenic carbonate and abundant mudstone (Jim Camp Wash beds), and an upper  
139 sandstone unit (Martha's Butte beds) (Martz and Parker, 2010). The five units are gradational,  
140 with the main variation being the abundance of mudstone in two of the middle units. A reddish  
141 siliceous horizon of uncertain regional extent has been recognized within the middle of the  
142 upper mudstone-rich unit in the CPCP-PFNP13-1A core. Similar horizons within other exposures  
143 of the Sonsela Member are marked by a significant die-off of the conifers that characterize  
144 Petrified Forest National Park (Creber and Ash, 1990), a turn-over of the vertebrate fauna  
145 (Parker and Martz, 2009, 2011), and perhaps a significant change in flora and paleoclimate  
146 (Reichgelt et al., 2013; Nordt et al., 2015; Baranyi et al., 2017). U-Pb (CA-TIMS/zircon) ages from  
147 the Sonsela Member range from ~220 to ~214 Ma (Ramezani et al., 2011; [Marsh et al., 2019](#);  
148 [Rasmussen et al., 202019](#)) from below the siliceous horizon and from ~214 to ~213 Ma  
149 (Ramezani et al., 2011; Nordt et al., 2015; Kent et al., 2018; [Rasmussen et al., 202019](#)) from  
150 above.

151 Overlying the conglomeratic sandstones of the Sonsela Member is a purplish mudstone that  
152 marks the base of the Petrified Forest Member (Fig. 2). This member consists of red and purple  
153 mudstone with abundant paleosols and pedogenic carbonate nodules, with local conglomeratic  
154 sandstone beds that formed in bedload-dominated streams. Near the top of the unit is the  
155 Black Forest bed, which consists of limestone-pebble conglomerate and reworked andesitic tuff  
156 (Ash, 1992). Zircon grains from the Black Forest bed have yielded U-Pb (ID-TIMS or CA-TIMS)  
157 ages of ~213 Ma to ~210 Ma (Riggs et al., 2003; Heckert et al., 2009; Ramezani et al., 2011; Kent  
158 et al., 2018; [Rasmussen et al., 202019](#)).

### 159 **3. SAMPLED HORIZONS**

160 We analyzed detrital zircon grains from twenty-nine samples collected from the Permian and  
161 Triassic strata described above. Samples include one from the Coconino Sandstone, five from  
162 the Moenkopi Formation (one that may be from the Wupatki Member and four from the  
163 Holbrook Member), and twenty-three from the Chinle Formation (one from the Mesa Redondo  
164 Member, three from the Blue Mesa Member, twelve from the Sonsela Member, and seven  
165 from the Petrified Forest Member). Approximate stratigraphic positions of the samples are  
166 shown on Figure 2, lithic characteristics are described in DR Table 1, and images of the sampled  
167 material (both core and thin sections) are presented in Appendix 1. Each sample consisted of 20  
168 cm (for sandstone) to 30 cm (for mudstone-siltstone) of  $\frac{1}{4}$  sections of the core.

### 169 **4. ANALYTICAL AND INTERPRETIVE METHODS**

170 Zircon mineral separation was performed at the Arizona LaserChron Center  
171 ([www.laserchron.org](http://www.laserchron.org)) using methods modified from those outlined by Gehrels (2000), Gehrels  
172 et al. (2008), and Gehrels and Pecha (2014) because of the small size of all samples and the  
173 abundance of clay minerals in many samples. The process included using a hand-crusher to  
174 break the samples apart, a gold pan for initial density separation, and an ultrasonic disruptor

175 (Hoke et al., 2014) to separate zircon crystals from clay mineral grains. Magnetic separation was  
176 performed with a Frantz Isodynamic separator, followed by density separation using methylene  
177 iodide.

178 Zircon grains greater than 60  $\mu\text{m}$  in size were enclosed in 1-inch epoxy mounts along with  
179 fragments of zircon standards SL (primary) and FC-1 and R33 (secondary). Mounts were  
180 polished approximately 5-10  $\mu\text{m}$  deep to expose the internal structure of the grains but retain  
181 as much material as possible for subsequent CA-TIMS analysis. Imaging was performed with a  
182 backscatter electron detector system (BSE) using a Hitachi S3400 scanning electron microscope  
183 (SEM) to ensure analysis of zircon and to avoid inclusions and fractures. Mounts were cleaned  
184 with 1% HCl and 1%  $\text{HNO}_3$  prior to isotopic analysis.

185 U-Pb isotopic analyses were conducted by LA-ICPMS using a Teledyne/Photon Machines  
186 Analyte G2 laser connected to a Thermo Element2 mass spectrometer. Analyses utilized a 20  
187  $\mu\text{m}$  diameter laser beam fired at 7 hz for 15 seconds, resulting in 10-12  $\mu\text{m}$  deep pits. Details of  
188 the analytical methods are reported in DR Table 2.

189 U-Pb ages are calculated with an in-house data-reduction routine (E2agecalc) following  
190 methods of Pullen et al. (2018). Analyses of zircon grains from our samples are reported in DR  
191 Table 3, with results filtered for discordance (using cutoffs of 80% and 105% concordance),  
192 precision (10%), and common Pb (>600 cps counts of 204). Following the recommendations of  
193 Horstwood et al. (2016), uncertainties for individual analyses include only internal (random or  
194 measurement) uncertainty contributions, whereas uncertainties of pooled ages contain both  
195 internal and external (systematic) contributions.

196 Detrital age distributions are displayed and analyzed with normalized probability density plots,  
197 which are based on the individual ages and measured uncertainties from each sample.  
198 Provenance interpretations are based on the main clusters of ages, with less emphasis on ages  
199 that do not belong to clusters given the possibility that they are unreliable due to Pb loss,  
200 inheritance, analysis of inclusions, high common Pb, or unusual Pb/U fractionation due to  
201 ablation along fractures (Gehrels, 2014).

202 Analysis of provenance is conducted by comparison with age distributions from five likely  
203 source regions for Permian-Triassic strata of the Colorado Plateau, which include the  
204 Appalachian orogen, the Ouachita orogen, local basement rocks of southwestern Laurentia, the  
205 East Mexico arc, and the Permian-Triassic magmatic arc developed along the Cordilleran margin  
206 of southwestern North America (Fig. 1; Dickinson, 2018). The age distributions for these regions  
207 include data from: (1) upper Paleozoic strata of the Appalachian foreland basin (Thomas et al.,  
208 2017) and Illinois and Forest City basins (Kissock et al., 2018), (2) upper Paleozoic strata of the  
209 Delaware (Xie et al., 2018), Fort Worth (Absalem et al., 2018), and Marathon (Thomas et al.,  
210 2019) basins, (3) lower Paleozoic strata of the Grand Canyon (Gehrels et al., 2011) and  
211 Cordilleran passive margin strata in southern California and northern Sonora (Gehrels and  
212 Pecha, 2014), (4) Permian and Triassic strata of the Barranca and El Antimonio Formations of

213 Sonora (Gonzalez-Leon et al., 2009; Gehrels and Pecha, 2014), Jura-Cretaceous strata of the  
214 Great Valley (DeGraaff-Surpless et al., 2002; Surpless et al., 2006; Wright and Wyld, 2007),  
215 Permian-Triassic igneous rocks in California (Chen and Moore, 1982; Miller et al., 1995; Tobisch  
216 et al., 2000; Barth and Wooden, 2006, 2011, 2013; Saleeby and Dunne, 2015), and (5) Mesozoic  
217 strata that accumulated adjacent to the East Mexico arc (Ortega-Flores et al., 2014). Age  
218 distributions for these five regions are presented in Figure 3.

219 Comparisons of age distributions are quantified using ~~several~~ two different statistical measures  
220 that examine the degree to which age distributions contain similar proportions of similar age  
221 groups. ~~Five metrics~~ used in this study include the ~~cross-correlation coefficient, values of~~  
222 ~~similarity and likeness, and the~~ Kolmogorov-Smirnov D (K-S-D) values and Kuiper-V values.  
223 The statistical basis as well as strengths and limitations of each of these metrics are  
224 summarized by Saylor and Sundell (2016) ~~and Wissink et al. (2018), and Vermeesch (2018a)~~.  
225 Results from these comparisons are presented in DR Table 4. The interpretations offered below  
226 are based on ~~cross-correlation~~ KS-D values ~~coefficients~~, although Kuiper-V values ~~all five metrics~~  
227 yield similar results. For both metrics, smaller values indicate a higher degree of similarity of  
228 age distributions. Comparisons are also presented visually through the use of multidimensional  
229 scaling (MDS) diagrams (Vermeesch, 2013; Saylor et al., 2017; Wissink et al., 2018), which  
230 provide a 2-dimensional representation of the differences between multiple age distributions.  
231 MDS analyses are ~~also~~ based on KS-D values ~~calculated from kernel density estimates (KDE's) of~~  
232 the age distributions ~~cross-correlation coefficients~~.

233 Maximum depositional ages (MDAs) are estimated from the youngest distinct cluster of ages in  
234 each sample (e.g., calculated from the age of the youngest distinct cluster of three or more  
235 overlapping ages Dickinson and Gehrels, 2009; Gehrels, 2014). The age of this cluster is  
236 estimated using ~~five~~ our different methods, each of which has strengths and limitations.  
237 Complications with these methods arise from (1) the need to make unconstrained decisions  
238 about which analyses to include or exclude from consideration, (2) the evidence that dates in  
239 some clusters have been compromised by Pb loss, resulting in dates that post-date deposition,  
240 (3) the evidence that some clusters also contain slightly older recycled grains that pre-date  
241 deposition, and (4) issues of statistical robustness for some methods (Vermeesch, 2018b).  
242 Following are short descriptions of the five ~~our~~ methods:

243 ~~•, as described below.~~

- 244 • Age of the youngest peak on a probability density plot (PDP). This method is advantageous  
245 because no decisions are made about which analyses are included/excluded, but it has the  
246 disadvantage that no uncertainty is reported for the peak age.
- 247 • Weighted Mean age and uncertainty of the youngest cluster. This method calculates the  
248 average age of a cluster by weighting each analysis according to the inverse-square of its  
249 uncertainty. The reported uncertainty relates to the mean age (e.g., standard error of the  
250 mean), not the age distribution of constituent analyses (e.g., standard deviation). An  
251 advantage of this method is that it also yields a Mean Square of the Weighted Deviates  
252 (MSWD), which is an indication of the degree to which the ages belong to a single

253 population (values of  $\sim 1$  or less indicate a single population). A disadvantage of this method  
254 is that the investigator must decide which ages are included in the calculation, which leads  
255 to the possibility of subjective bias. In this study, clusters include the main set of continuous  
256 ages, with boundaries selected at the youngest and oldest gap in ages. This calculation is  
257 available from the Weighted Mean function in Isoplot (Ludwig, 2008).

- 258 • Tuffzirc age and uncertainty of the youngest cluster. This method uses the age extractor  
259 function in Isoplot (Ludwig, 2008), which identifies the largest cluster of ages that overlap to  
260 an acceptable degree (probability-of-fit  $> 0.05$ ), reports the median value as the most likely  
261 age, and uses the range of included ages to calculate an asymmetric uncertainty. The  
262 reported uncertainty refers to the median value (not the range of constituent analyses).  
263 Excluded ages are interpreted to pre-date the selected cluster (if older), or to be  
264 compromised by Pb loss (if younger). This method is advantageous in that no subjective  
265 decisions are made about including/excluding ages.
- 266 • Maximum Likelihood age and uncertainty. This method uses a maximum likelihood analysis  
267 to determine the gaussian distribution that best fits the youngest cluster. The reported  
268 uncertainty refers to the most likely value (not the range of constituent analyses). This  
269 method is advantageous in that no subjective decisions are made about including/excluding  
270 ages. It is available from the Unmix function of Isoplot (Ludwig, 2008).

271

272 Finally, we also use the minimum age model of Galbraith and Laslett (1993) and Vermeesch  
273 (2020). This method assumes that a set of dates is a mixture of a discrete young component  
274 and a continuous older component. It uses the method of maximum likelihood to determine  
275 the age and uncertainty of the younger component. Calculations were conducted using IsoplotR  
276 (Vermeesch, 2018b), which returns the minimum age and also a central age that is similar to  
277 the weighted mean described above.

278

279

280 The results of these calculations are presented in DR Tables ~~3 and 6~~. Shown separately are  
281 estimates from the first four methods noted above, and the average of these four estimates, as  
282 well as the minimum age (and uncertainty) which we interpret as the maximum depositional  
283 age.

284

285 DR Table 6 also reports the age and uncertainty of the youngest analysis from each sample. This  
286 youngest age does not provide a reliable maximum depositional age given that the youngest  
287 age of a distribution will always be younger than the true age due to analytical uncertainty  
288 (Gehrels, 2014). For example, as described by Coutts et al. (2019), consider the analytical data  
289 from a population of zircon grains that have exactly the same true age. Because of analytical  
290 uncertainty, the measured ages of half of the analyses will be younger than the true age, and  
291 half will be older, and the youngest age will be significantly younger than the mean (true) age.  
292 Ironically, the more grains analyzed, the greater the inaccuracy of this youngest age  
293 (Vermeesch, 2020)!

294 In addition to this statistical bias, the youngest single age will be even farther from the mean  
295 (true) age if it has been compromised by Pb loss (e.g., Andersen et al., 2019). We report these  
296 youngest ages because they provide important information about the possibility that analyses  
297 included in the youngest cluster have also experienced Pb loss. DR Table 6 accordingly reports  
298 this youngest age (and uncertainty), as well as information about its U concentration, the  
299 average U concentration of the youngest cluster of ages, and whether the youngest age belongs  
300 to the youngest cluster or is an outlier (based on Tuffzirc analysis). U concentration is important  
301 because Pb loss is commonly correlated with the degree of radiation damage, which is a  
302 function of U concentration (and age).

303 A second test of the likelihood that analyses belonging to the youngest cluster have  
304 experienced Pb loss is provided by a plot of U concentration versus age for analyses belonging  
305 to the youngest cluster. Such plots are shown for every sample in DR Table 3, and whether a  
306 correlation exists is indicated in DR Table 6.

307 ~~Also included in DR Table 6 are the preferred MDA age and uncertainty for each sample. The~~  
308 ~~preferred age is based on the average of the four age estimates s determined by peak age,~~  
309 ~~weighted mean, Tuffzirc, and Unmix analyses. The uncertainty of this preferred age is based on~~  
310 ~~the average of the uncertainty from each method, and is shown with both internal-only~~  
311 ~~uncertainties and with combined internal and external uncertainties.~~

312 The average precision of individual analyses reported herein is 2.3% ( $2\sigma$ ) for  $^{206}\text{Pb}^*/^{238}\text{U}$  dates  
313 and 2.6% for  $^{206}\text{Pb}^*/^{207}\text{Pb}^*$  dates. For pooled ages, calculated as described above, the average  
314 precision is 0.52% ( $2\sigma$ ) including only internal uncertainties and 0.98% ( $2\sigma$ ) including both  
315 internal and external sources of uncertainty. The accuracy of our analyses can be estimated  
316 from the age of the secondary standards that were analyzed with each set of unknowns. As  
317 reported in DR Table 7 and shown on Figure 4, sets of  $^{206}\text{Pb}^*/^{238}\text{U}$  dates for FC-1 are offset  
318 between +0.25% and -0.45% from the reported  $^{206}\text{Pb}^*/^{238}\text{U}$  date of 1099.9 Ma (Paces and  
319 Miller, 1993), with an average offset for all 1,065 analyses of +0.03%. For R33, offsets range  
320 from +0.85% to -0.95% from the assumed age of 419.3 Ma (Black et al., 2004), with an average  
321 offset for all 291 ages of -0.23%. MSWD values for the sets of FC-1 and R33 ages are 0.95 and  
322 0.92 (respectively) – this demonstrates that reported uncertainties for individual analyses are  
323 accurate, and that MSWD values for sets of unknown ages are reliable indicators of the  
324 existence of multiple age components.

325 Interpretation of our ages relative to the Geologic Time Scale is based on the August 2018  
326 version of the International Chronostratigraphic Chart (Cohen et al., 2013).

327 U-Pb geochronology by LA-ICPMS also provides U concentrations and U/Th values for each  
328 analysis, which can be used as a geochemical fingerprint of detrital zircon grains (e.g., Gehrels  
329 et al., 2006, 2008; Riggs et al., 2012, 2016). This information is accordingly reported for each  
330 analysis in DR Table 3, and for each set of analyses in DR Table 6.

## 331 5. U-Pb GEOCHRONOLOGIC RESULTS

332 Results of our U-Pb geochronologic analyses are described below, keyed to the age  
333 distributions for individual samples that are shown on Figures 5, 6, and 7. Figure 8 presents age  
334 distributions for combined sets of samples. Age distributions from all of the samples are  
335 compared statistically in DR Table 4 using the five metrics described above, and MDS plots are  
336 shown in Figure 9.

337 We note that Rasmussen et al. (2020~~19~~) have reported a subset of the LA-ICPMS ages  
338 presented herein. The ages reported in their study are for the grains selected for CA-TIMS  
339 analysis, which in most cases are among the youngest grains in each of our samples (as  
340 documented in Appendix 2). This strategy was followed assuming that these grains represent  
341 the youngest age components in each sample, and accordingly provide the most useful  
342 maximum depositional ages. The individual dates reported in the two studies are identical, but,  
343 given the selection process noted above, the pooled ages reported by Rasmussen et al.  
344 (2020~~19~~) are consistently younger than the pooled ages reported herein. A comparison of the  
345 results of the two studies is summarized in Appendix 2. The discussions below are based on the  
346 full set of ages from each sample.

347 Sample numbers are registered to the CPCP core (CPCP-PFNP13-1A) by the number of the core  
348 run and segment (e.g., our sample number 383-2 is from CPCP-PFNP13-1A-383Y-2, which  
349 specifies that the material is from run 383, segment 2). The part of each segment that was  
350 collected for geochronologic analysis is specified in DR Table 1.

### 351 5.1 Coconino Sandstone

352 Our sample from quartz arenite of the lower Permian (Leonardian) Coconino Sandstone  
353 (sample 390-1) yielded 285 acceptable ages (DR Table 3; Figure 4). Most grains belong to two  
354 broad age groups of ~2.0-1.0 Ga and ~640-295 Ma. Individual age peaks are at 2712, 1898,  
355 1746, 1646, 1497, 1432, 1347, 1162, 1038, 667, 612, 590, 552, 476, 430, 419, 391, 374, 355,  
356 341, and 300 Ma.

### 357 5.2 Moenkopi Formation

358 Five samples from the Lower-Middle Triassic Moenkopi Formation have been analyzed (Fig. 2).  
359 The lowest sample (383-2) is assigned to the Wupatki Member based on the red-brown  
360 laminated mudstone to fine-grained sandstone lithology (Fig. 2; Table DR 1). The age  
361 distribution from this sample is very similar to that found in underlying upper Paleozoic strata,  
362 with two dominant age groups from ~2.2 Ga to 1.0 Ga and from ~680 Ma to 250 Ma (Fig. 5).  
363 Although the preferred interpretation for this sample is that it belongs to the lowest part of the  
364 Moenkopi Formation, an alternative is that the sample is late Paleozoic in age, and perhaps  
365 correlative with fine-grained clastic strata (e.g., the Toroweap Formation) that regionally overlie  
366 the Coconino Sandstone. In an effort to provide a comparison with underlying and overlying  
367 strata, the results from this sample are shown on Figures 5 and 6. Additional studies of the

368 sampled horizon are needed to resolve whether this sample belongs to the Moenkopi  
369 Formation or underlying upper Paleozoic strata.

370 The upper four samples (349-3, 335-1, 327-2, and 319-2) are all from sandstone, siltstone, and  
371 mudstone of the Holbrook Member. These samples yield generally similar age distributions  
372 (average KS-D values CCC of 0.1924; DR Table 4), with significant proportions of ~1.42 Ga, 650-  
373 510 Ma, 290-270 Ma, and 250-235 Ma ages (Fig. 6). With ages from all four Moenkopi  
374 Formation samples combined, PDP peak ages are 1420, 594, 543, 285, and 250 Ma (Fig. 8). ~~As  
375 shown in Figures 9B and 9C, age distributions from the lower two samples (349-3 and 335-1)  
376 and upper two samples (327-2 and 319-2) form two distinct groups. These clusters are also  
377 apparent from CCC values of 0.83 and 0.24 for the lower and upper samples (respectively), in  
378 comparison with a low average value (0.08) for comparison of the two sets with each other (DR  
379 Table 4).~~

### 380 **5.3 Chinle Formation**

381 Twenty-three samples from the Mesa Redondo Member, Blue Mesa Member, Sonsela Member,  
382 and Petrified Forest Member of the Chinle Formation have been analyzed (Fig. 2). Results from  
383 each member are described separately below.

#### 384 **5.4 Mesa Redondo Member**

385 One sample of sandstone from the Mesa Redondo Member (305-2) yields dominant age groups  
386 of ~2.0-1.6 Ga, 1.44 Ga, 1.1-1.0 Ga, 750-500 Ma, and 450-300 Ma, and 290-220 Ma (Fig. 7), with  
387 PDP peak ages of 1443, 1036, 618, 412, 323, 248, and 223 Ma. As reported in DR Table 4 and  
388 shown on Figure 9B and 9C, the >240 Ma ages in this sample resemble ages in the underlying  
389 Moenkopi Formation and Coconino Sandstone.

#### 390 **5.5 Blue Mesa Member**

391 Three samples (297-2, 287-2, 261-1) of siltstone and mudstone from the Blue Mesa Member  
392 yield similar results, with nearly identical <240 Ma ages and small but varying proportions of  
393 ~1.64 Ga, 1.44 Ga, 1.1-1.0 Ga, 650-500 Ma, and 440-240 Ma ages (Figures 7 and 8). Both <240  
394 Ma ages (Fig. 9A) and >240 Ma ages (Fig. 9C) differ from those in underlying strata of the Mesa  
395 Redondo Member. Between 56% and 89% of the grains analyzed from these samples yield ages  
396 between 232 and 210 Ma, with PDP peak ages of 221-220 Ma (Fig. 7; DR Table 6). With all three  
397 samples combined, 62% of the ages are <240 Ma, and PDP peak ages are 1630, 1440, and 220  
398 Ma (Fig. 8).

#### 399 **5.6 Sonsela Member**

400 Twelve samples (243-3 to 158-2) from the Sonsela Member yield two different sets of age  
401 distributions (Figures 7, 8, and 9; DR Table 3). The lower six samples (243-3 to 196-3), all  
402 consisting of sandstone and subordinate siltstone (DR Table 1), yield small numbers of  
403 Precambrian grains that are mostly ~1.65 and 1.44 Ga, with few ~1.1-1.0 Ga grains. These



404 samples yield between 53% and 79% ages <240 Ma, with most ages between 234 and 208 Ma,  
405 and PDP peak ages of 221-218 Ma (Fig. 7). With ages from all six samples combined, 68% of the  
406 grains are <240 Ma, and PDP peak ages are 1650, 1445, 1084, and 219 Ma (Fig. 8). Comparison  
407 of age distributions (Figures 7 and 8), KS-D values (DR Table 4), and MDS patterns (Fig. 9)  
408 suggests that the <240 Ma ages in lower Sonsela Member these strata are similar to  
409 indistinguishable from <240 Ma ages in underlying Blue Mesa strata, whereas >240 Ma ages in  
410 the two sets of samples are less similar due to the variability of ages from the three Blue Mesa  
411 Member samples. Ages that are >240 Ma in these strata have even less similarity to ages from  
412 the Mesa Redondo Member, Moenkopi Formation, and Coconino Sandstone (Fig. 9; DR Table  
413 4).

414 The upper six samples from the Sonsela Member (195-2 to 158-2) consist mainly of sandstone  
415 and subordinate siltstone (DR Table 1). All six samples yield a subordinate but consistent  
416 proportion of Precambrian ages that are mostly ~1.43 and 1.1-1.0 Ga, with few 1.65 Ga grains  
417 (Fig. 7). Grains with ages of <240 Ma comprise between 39% and 77% of the grains analyzed.  
418 These ages are somewhat younger than in lower Sonsela Member samples, with PDP peak ages  
419 of 217-214 Ma. With all six samples combined, 50% of the grains are <240 Ma, and PDP peak  
420 ages are 1643, 1434, 1082, 256, and 215 Ma (Fig. 8).

421 Statistical analysis (MDS patterns in Figure 9 and KS-D values in DR Table 4) shows that the  
422 <240 Ma ages in upper and lower Sonsela Member strata are significantly different, whereas  
423 >240 Ma ages are less distinct. Exceptions to this are >240 Ma ages in sample 243-3 (lower  
424 Sonsela Member), which resemble equivalent ages in strata of the upper Sonsela Member (Fig.  
425 9C), and <240 Ma ages in sample 196-3, which share characteristics with strata of both the  
426 upper and lower Sonsela Member (Fig. 9A). Ages from strata of the upper Sonsela Member  
427 show even less overlap with ages from strata of the Blue Mesa Member and underlying units  
428 (Fig. 9 and DR Table 4).

### 429 **5.7 Petrified Forest Member**

430 Seven samples (131-2 to 52-2) from the Petrified Forest Member were collected mainly from  
431 claystone, mudstone, siltstone, and fine-grained sandstone, with only the lowest sample (131-  
432 2) consisting of coarse-grained sandstone. The upper six fine-grained samples yield between  
433 17% and 72% <240 Ma ages that are significantly younger than in underlying strata, with PDP  
434 peak ages between 212 and 209 Ma. Ages that are >240 Ma in most of these samples differ  
435 from equivalent ages in strata of the Blue Mesa Member and Sonsela Member, but overlap to  
436 varying degrees with ages in strata of the Mesa Redondo Member, Moenkopi Formation, and  
437 Coconino Sandstone (Fig. 9C; DR Table 4). With the six samples combined, 35% of the grains are  
438 <240 Ma, and PDP peak ages are 1636, 1430, 1032, 629, 379, 287, and 209 Ma (Fig. 8). The  
439 lowest sample (131-2), consisting of coarse-grained sandstone, differs from the other Petrified  
440 Forest Member samples, with an age peak of 221 Ma, and a greater proportion (68%) of >240  
441 Ma ages (Fig. 7). The <240 Ma ages are very similar to equivalent ages in strata of the lower  
442 Sonsela Member (Fig. 9A; KS-D=0.1297), whereas >240 Ma ages are slightly more similar to

443 ages in the upper Sonsela Member ( $\text{CCCKS-D}=0.1772$ ) than in the lower Sonsela Member ( $\text{KS-}$   
444  $\text{DCCC}=0.2259$ ) (Fig. 9C).

### 445 **5.8 Summary of Chinle results**

446 The patterns of LA-ICPMS ages described above suggest that the studied part of the Chinle  
447 Formation comprises four different units, each of which has a distinct chronologic signature for  
448 both <240 Ma and >240 Ma ages (Fig. 8). These chronostratigraphic units correspond to the  
449 Mesa Redondo Member, Blue Mesa Member and lower part of the Sonsela Member, upper  
450 part of the Sonsela Member, and Petrified Forest Member.

## 451 **6. U AND Th GEOCHEMISTRY OF CHINLE ZIRCON GRAINS**

452 In an effort to evaluate whether the Triassic zircon grains from the four chronostratigraphic  
453 units also have distinct chemical signatures [following Riggs et al. (2012, 2016)], Figure 10  
454 summarizes the U concentrations and U/Th values for Triassic zircon grains analyzed from each  
455 unit. The patterns exhibited in these plots suggest that (1) zircon grains from the Mesa  
456 Redondo Member are significantly different from zircon grains in overlying strata, (2) grains in  
457 strata of the Blue Mesa Member and lower Sonsela Member differ from grains in overlying  
458 strata of the upper Sonsela Member and Petrified Forest Member, and (3) grains in strata of the  
459 upper Sonsela Member and Petrified Forest Member have distinctive and slightly different  
460 bimodal patterns. Plots showing U concentrations and U/Th values for individual samples are  
461 included in DR Table 3.

## 462 **7. PROVENANCE INTERPRETATIONS**

463 Detrital zircon geochronology has previously been used to reconstruct the provenance of  
464 Permian and Triassic strata of the Colorado Plateau by Riggs et al. (1996, 2003, 2012, 2013,  
465 2016), Dickinson and Gehrels (2003, 2008), Gehrels et al. (2011), Lawton et al. (2015), and  
466 Marsh et al. (2019). The results of most of these ~~chronological~~[geochronologic](#) studies, and a  
467 large number of stratigraphically based analyses, have recently been summarized by Dickinson  
468 (2018). The following sections compare our new results with this existing information.

469 The following comparisons are based in part on qualitative comparison of age distributions of  
470 the strata that we have analyzed and of age distributions from five potential source areas  
471 (summarized on Figure 3). As described by Gehrels (2000), such comparisons focus on the  
472 degree to which two age distributions contain similar proportions of similar ages. Comparisons  
473 are also based on the results of statistical analyses (DR Table 4) that compare our results with  
474 the age distributions of possible source areas, and on graphic displays of these comparisons  
475 using MDS plots (Fig. 9).

### 476 **7.1 Coconino Sandstone**

477 Lawton et al. (2015) and Dickinson (2018) suggest that lower Permian strata of the Colorado  
478 Plateau comprise a regional blanket of eolian strata that was shed predominantly from the

479 Appalachian and/or Ouachita orogens, with increasing input in northern regions from local  
480 basement rocks exposed in the Uncompahgre or Ute Uplift (Fig. 1). These interpretations are  
481 supported by the age distributions shown on Figures 5 and 11, with southern strata (Coconino,  
482 Cedar Mesa, and White Rim sandstones) forming a distinct group dominated by  
483 Appalachian/Ouachita detritus, and northern strata (Castle Valley and Cutler strata) forming a  
484 separate group with increasing proportions of ca 1.44 Ga grains. The age distribution from our  
485 Coconino Sandstone sample (390-1) fits well with other strata from the southern Colorado  
486 Plateau in having abundant 1.2-1.0 and 670-300 Ma (Appalachian-Ouachita) grains and a low  
487 proportion of ~1.44 Ga grains (Figures 5 and 11; DR Table 4).

## 488 7.2 Moenkopi Formation

489 As summarized on Figure 6, the detrital zircon ages from our four Holbrook Member samples  
490 are generally similar to ages from a Holbrook Member sandstone reported by Dickinson and  
491 Gehrels (2008). Dominant >300 Ma age groups and interpreted source terranes include ~1.44  
492 Ga and subordinate ~2.0-1.6 Ga grains derived from Laurentian Precambrian basement and  
493 ~670-300 Ma grains derived from Ouachita/Gondwana sources. Based on comparison with  
494 detrital zircon ages from strata that accumulated in proximity to the East Mexico and southern  
495 Cordilleran arcs (Fig. 3), 300-260 Ma grains (PDP peak ages of 285, 284, 265, 260, and 279) are  
496 interpreted to have been shed from the East Mexico arc (peak age of 284 Ma), whereas 260-  
497 230 Ma grains (peak ages of 250, 248, 228, 245, and 239 Ma) were likely shed from Early-  
498 Middle Triassic parts of the Cordilleran magmatic arc in California and northwestern Mexico  
499 (peak ages of 243, 236, and 226 Ma) (Fig. 3). Statistical analyses (DR Table 4) suggest nearly  
500 equal contributions from the Ouachita orogen, local basement rocks, and the East Mexico arc.

501 More detailed analysis of the age distributions (Fig. 6) and MDS patterns (Fig. 9) suggest that  
502 the lower two samples (349-3 and 335-1) [plus sample CP8 of Dickinson and Gehrels (2008)] are  
503 dominated by ~1.44 Ga and ~285 Ma grains, whereas the upper two samples (327-2 and 319-2)  
504 are dominated by ~620-590 Ma and ~250-230 Ma grains. The age distributions (Fig. 6) and  
505 comparison metrics (Fig. 9C; DR Table 4) suggest that the lower samples were shed mainly from  
506 local basement rocks (CECKS-D=0.350) and the East Mexico arc (CCC=0.22), whereas the upper  
507 samples were shed largely from the Ouachita orogen (CECKS-D=0.23).

## 508 7.3 Chinle Formation

509 Our results from detrital zircon grains recovered from strata of the Chinle Formation are  
510 consistent with the provenance and paleogeographic reconstructions offered by Riggs et al.  
511 (1996, 2003, 2012, 2013, 2016), Dickinson (2018), and Marsh et al. (2019). Given the observed  
512 age distributions (Fig. 7) and the location of our study site relative to Late Triassic  
513 paleogeographic and paleotectonic features of southwestern North America (Fig. 12), likely  
514 sources for pre-Triassic grains include rocks exposed in the Ouachita orogen to the southeast  
515 and the Ancestral Mogollon highlands to the south and southwest. Given the abundance of ash  
516 layers, bentonitic mudstone, and near-depositional-age zircon grains in strata of the Chinle

517 Formation, and the existence of arc-related plutons and volcanic rocks of Triassic age in Sonora  
518 and southern California (Barth and Wooden, 2006, 2011, 2013; Saleeby and Dunne, 2015; Riggs  
519 et al., 2016), Stewart et al. (1986), Riggs et al. (2012, 2016), Dickinson (2018), Marsh et al.  
520 (2016), and many other researchers conclude that Triassic grains in Chinle strata were derived  
521 from the active arc built along the southern Cordilleran margin. The occurrence in fore-arc and  
522 back-arc strata of very similar distributions of ages (Fig. 3) is inconsistent with interpretations  
523 (e.g., Hildebrand, 2009, 2013) that the early Mesozoic arc was located far from southwestern  
524 North America.

525 Although our data are entirely consistent with the provenance interpretations outlined above,  
526 the density of our sampling and the large number of analyses from most samples provide  
527 opportunities to reconstruct temporal changes in Triassic provenance in greater detail, and with  
528 the benefit of statistical analyses to quantify conclusions. Following are interpretations based  
529 on strata belonging to each of the different members of the Chinle Formation.

#### 530 **7.4 Mesa Redondo Member**

531 The provenance of strata belonging to the Mesa Redondo Member is similar to that of the  
532 underlying Moenkopi Formation, with our sample (305-2) containing abundant ~640-300 Ma  
533 grains derived from Ouachita/Gondwana sources as well as ~290-260 Ma grains derived from  
534 the East Mexico arc (Fig. 8). Statistical analysis confirms higher similarity of >240 Ma grains with  
535 Ouachita sources (0.58) than with Appalachian (0.35) or local basement (0.15) sources (DR  
536 Table 4). This sample also yields a significant proportion of Triassic ages that approximate the  
537 depositional age for these strata (Fig. 7). These young grains, with a PDP age peak of 223 Ma,  
538 are interpreted to have been transported primarily by aeolian processes from the active  
539 magmatic arc to the west (Fig. 12). Statistical analysis demonstrates that the Triassic ages in  
540 these samples are significantly different from ages in overlying strata (Fig. 9A) and that the  
541 >240 Ma ages are similar to those in some strata of the Petrified Forest Member (Fig. 9C).

#### 542 **7.5 Blue Mesa Member**

543 Our three samples from strata of the Blue Mesa Member yield a large proportion of Triassic  
544 zircon grains (Figures 7 and 8) that were derived from the active Cordilleran magmatic arc to  
545 the west (Fig. 12), and a small proportion of pre-240 Ma grains that were shed from local  
546 basement rocks and the Ouachita and/or Appalachian orogens (Fig. 8). Statistical analysis  
547 confirms that the Triassic ages in all these samples are quite similar (Fig. 9A), whereas the age  
548 distributions of >240 Ma grains in the three samples are more variable (Fig. 9C; DR Table 4).

#### 549 **7.6 Lower Sonsela member**

550 The lower six samples from the Sonsela Member yield a large proportion of Triassic grains  
551 derived from the Cordilleran magmatic arc, and fewer ages derived from local basement rocks  
552 and Ouachita/Gondwana sources (Figures 7 and 8). Distinctive among the older grains is a  
553 significant proportion of ~1.44 Ga grains that most likely may have been incorporated during

554 ~~transport from the Ouachita orogenic highlands, or may~~ signal increased input from the  
555 Ancestral Mogollon highlands to the southwest (Marsh et al., 2019) (Fig. 12). MDS analysis  
556 demonstrates that the <240 Ma and >240 Ma ages in these samples are quite similar, with the  
557 ~~only significant~~ main difference being the larger number of ~1.1 Ga grains in sample 243-3  
558 (Figures 7 and 9C).

### 559 **7.7 Upper Sonsela Member**

560 The upper six samples from the Sonsela Member reveal a continued low contribution from the  
561 Ouachita orogen, and a significant increase in the proportion of ~1.08 Ga and 260-240 Ma  
562 grains (Figures 7 and 8). The ~260-240 Ma grains were likely derived from Permian-Early Triassic  
563 igneous rocks along the southern Cordilleran margin (Saleeby and Dunne, 2015; Riggs et al.,  
564 2016), exposed in the Ancestral Mogollon Highlands (Fig. 12). The prominent ~1.44 and 1.08 Ga  
565 grains in these samples may also have been shed from highland sources to the south and  
566 southwest. Triassic grains in these samples record a slightly younger (230 to 204 Ma, peak age  
567 of 215 Ma) phase of magmatism along the Cordilleran margin. Significant changes in both <240  
568 Ma and >240 Ma ages occur between samples 196-3 and 195-2 (Figure 7). MDS analysis  
569 demonstrates that patterns of both <240 Ma and >240 Ma ages are consistent among the six  
570 upper Sonsela Member samples, but are distinct from ages in all other parts of the Chinle  
571 Formation (Figures 7 and 9).

### 572 **7.8 Petrified Forest Member**

573 Strata of the Petrified Forest Member record an important shift in provenance, with  
574 significantly greater detrital input from the East Mexico arc (~287 Ma) and the Ouachita orogen  
575 (~640-300 Ma), and a broader range of >1.0 Ga basement sources (Figures 7 and 8). Triassic  
576 grains in these strata are also significantly younger, with ages of 228 to 200 Ma (peak age of  
577 209 Ma).

578 An exception to these patterns is recorded by ages from the coarse-grained sandstone of  
579 sample 131-2, which has Precambrian grains that are mainly ~1.1-1.0 and 1.44 Ga (like upper or  
580 lower Sonsela Member; Fig. 9CB), and Triassic grains that are ~221 Ma (like strata of the lower  
581 Sonsela Member and Blue Mesa Member; Fig. 9A). This lower Petrified Forest Member sample  
582 is interpreted to have been reworked mainly from lateral equivalents of underlying strata of the  
583 Sonsela Member and Blue Mesa Member, with little or no input from the active arc to the west.  
584 ~~MDS analysis shows that sample 116-1 contains a mix of these older reworked grains and the~~  
585 ~~younger grains present in overlying strata (Fig. 9A).~~

## 586 **8. MAXIMUM DEPOSITIONAL AGES**

587 The depositional age of Triassic strata on the Colorado Plateau is of considerable interest  
588 because of the rich faunal and paleoclimatic records preserved within the Moenkopi Formation  
589 and Chinle Formation, and as the zircon-based geochronological framework for the early  
590 Mesozoic when coupled with paleomagnetic polarity stratigraphy and astrochronology (Olsen

591 et al., 2018, 2019; Kent et al., 2018, 2019; Rasmussen et al., 202019). There accordingly have  
592 been many prior attempts to determine the depositional age of these strata by dating igneous  
593 zircon grains in ash beds or volcanic cobbles and detrital zircon grains in clastic strata (e.g.,  
594 Riggs et al., 1996, 2003, 2012, 2013, 2016; Heckert et al., 2009; Dickinson and Gehrels, 2009;  
595 Irmis et al., 2011; Ramezani et al., 2011, 2014; Atchley et al., 2013; Nordt et al., 2015). As part  
596 the Colorado Plateau Coring Project, Kent et al. (2018) and Rasmussen et al. (202019) report  
597 the results of CA-TIMS analyses on many of the same samples reported herein. All of the  
598 available CA-TIMS ages, and the preferred age models of Kent et al. (2019) and Rasmussen et al.  
599 (202019), are shown on Figure 13.

600 ~~Maximum depositional ages (MDA's) have been estimated calculated from the LA-ICPMS ages~~  
601 ~~using four different methods (described above), with results presented in DR Tables 3 and 6 and~~  
602 ~~shown graphically on Figure 13. We use the average of the youngest probability peak, tuffzirc,~~  
603 ~~unmix, and weighted mean results to estimate the age of all dates belonging to the youngest~~  
604 ~~cluster. In the following discussion we assume that the average of the ages and uncertainties~~  
605 ~~calculated using these four different methods yields the most reliable maximum depositional~~  
606 ~~age available from our LA-ICPMS data. These average (or preferred) ages are reported in DR~~  
607 ~~Table 6, shown on Figure 13, and described below with 2 $\sigma$  uncertainties incorporating only~~  
608 ~~internal contributions (for inter-sample comparison) and incorporating both internal and~~  
609 ~~external uncertainty contributions (for comparison with ages from other studies) (e.g., 224.4  $\pm$~~   
610 ~~2.0/2.7 Ma).~~

611 Maximum depositional ages (MDA's) have been determined using the minimum age model of  
612 Vermeesch (2020). The possibility that ~~this estimated~~ a maximum depositional age has been  
613 compromised by Pb loss is evaluated mainly by determining whether there is a correlation  
614 between U concentration and age. One criterion is whether the youngest single age has higher  
615 U concentration than the average of the youngest cluster – if yes than the youngest analysis  
616 (and perhaps other analyses within the youngest cluster) may have experienced Pb loss. A  
617 second criterion is whether analyses within the youngest cluster display an inverse correlation  
618 between U concentration and age – if yes, then the higher U and younger analyses within the  
619 cluster may have experienced Pb loss. An additional criterion is whether the youngest date is  
620 excluded from the cluster determined by Tuffzirc analysis. Samples in which all three methods  
621 suggest the presence of Pb loss are shown with red arrows on Figure 13. Rasmussen et al.  
622 (202019) document Pb loss in zircon grains from several of our samples by showing that CA-  
623 TIMS ages are commonly older than LA-ICPMS ages from the same crystals.

624 ~~Evidence for Pb loss is shown on Figure 13 with small arrows adjacent to the MDA's, with the~~  
625 ~~number of arrows showing the number of lines of evidence supporting Pb loss.~~

## 626 **8.1 Coconino Sandstone**

627 Our analyses do not provide a useful ~~MDA~~ maximum depositional age for strata of the Coconino  
628 Sandstone (sample 390-1) because few late Paleozoic ages were recovered from this sample.

## 629 8.2 Holbrook Formation of the Moenkopi Formation

630 Of our four samples from the Holbrook Member of the Moenkopi Formation, three yield  
631 ~~preferred~~MDA's that young upward from  $248.059 \pm 1.821.6/2.5$  Ma to  $246.638.4 \pm$   
632  $1.922.0/2.8$  Ma to  $236.78245.7 \pm 9.921.9/2.7$  Ma (DR Table 6). These MDA's are consistent  
633 with the inferred Early-Middle Triassic age of the strata and the corresponding ~251-237 Ma  
634 range for Early and Middle Triassic time on the Geologic Time Scale (Cohen et al., 2013). All  
635 three samples show patterns of U concentration that suggest the possibility of ~~minor~~Pb loss  
636 (DR Table 6).

## 637 8.3 Mesa Redondo Member of the Chinle Formation

638 Our one sample (305-2) from strata of the Mesa Redondo Member yields an ~~preferred~~ MDA of  
639  $223.243 \pm 1.503/2.2$  Ma (DR Table 6). ~~s that all ages belong to the same age population, and~~  
640 ~~p~~Patterns of U concentration do not indicate the presence of Pb loss (DR Table 6). This MDA  
641 overlaps with CA-TIMS ages of ~224.7-221.7 Ma from the same sample but is slightly older than  
642 the preferred single-grain age of ~221.7 Ma (Rasmussen et al., 20202019). ~~However, t~~The LA-  
643 ICPMS MDA of  $223.243 \pm 1.503/2.2$  is ~~significantly~~ younger than CA-TIMS ages of ~225.2 Ma  
644 (Ramezani et al., 2011) and ~227.6 (Atchley et al., 2013) from outcrop samples of the Mesa  
645 Redondo Member.

## 646 8.4 Blue Mesa Member of the Chinle Formation

647 Our three samples (297-2, 287-2, 261-1) from strata of the Blue Mesa Member yield ~~preferred~~  
648 MDA's of  $219.68220.6 \pm 0.460.6/2.1$ ,  $218.62220.2 \pm 0.981.01.3/2.2$ , and  $2210.237 \pm 1.021.3/1.9$   
649 Ma (DR Table 6). All samples yield MSWD values >1.0 (average of 2.4), which indicates  
650 ~~documents~~ the presence of multiple age populations and/or Pb loss (DR Table 6). Patterns of U  
651 concentration suggest the possible presence of Pb loss in all three samples, and likely Pb loss in  
652 sample 287-2. As shown on Figure 13, these MDA's ages are slightly younger than similar to  
653 most CA-TIMS ages from strata of the Blue Mesa Member. From lower strata, our ages are  
654 slightly younger than a CA-TIMS age of ~221.8 Ma [from sample 297-2; Rasmussen et al.  
655 (202019)], and indistinguishable from a CA-TIMS age of ~220.5 Ma [from sample 287-2;  
656 Rasmussen et al. (202019)], and similar to an ID-TIMS age of ~220.9 Ma [from outcrop; Heckert  
657 et al. (2009)]. From upper strata, our age is similar to a CA-TIMS age from outcrop of ~220.1 Ma  
658 (Atchley et al., 2013) but significantly younger than a CA-TIMS age of ~223.0 Ma (Ramezani et  
659 al., 2011), also from outcrop.

## 660 8.5 Lower part of the Sonsela Member

661 Our six samples from the lower part of the Sonsela Member (243-3 to 196-3) yield ~~preferred~~  
662 MDA's of  $219.27 \pm 0.44220.3 \pm 0.9/1.8$  Ma (sample 243-3),  $220.81 \pm 0.44220.6 \pm 0.5/1.8$  Ma  
663 (sample 227-3),  $221.30 \pm 0.48220.5 \pm 0.6/1.6$  Ma (sample 215-2),  $219.21 \pm 0.66220.9 \pm 0.7/2.3$  Ma  
664 (sample 210-1), and  $221.06 \pm 0.50220.6 \pm 0.6/1.7$  Ma (sample 201-1). The sixth, uppermost  
665 sample (196-3) yields younger ages with an ~~preferred~~ MDA of  $217.93 \pm 0.56218.2 \pm 0.7/1.6$  Ma.

666 MSWD values for these samples are all high (average of 2.6), which demonstrates the presence  
667 of multiple age components. There is evidence for Pb loss in analyses from samples 243-3 and  
668 210-1.

669 As shown on Figure 13, these MDA's are 1-3 m.y. older than most CA-TIMS ages from  
670 equivalent strata. From oldest to youngest, the CA-TIMS ages include ~220.1 Ma [from outcrop;  
671 Atchley et al. (2013)] from near the base, through ~218.8 Ma [sample 243-3; Rasmussen et al.  
672 (202019)], ~217.7 Ma [sample 227-3; Rasmussen et al. (202019)], ~219.3 Ma [from outcrop;  
673 Ramezani et al. (2011)], ~217.8 Ma [sample 215-2; Rasmussen et al. (202019)], ~218.0 Ma [from  
674 outcrop; Ramezani et al. (2011)], and ~215.7 Ma and 214.4 Ma [samples 201-1 and 196-3;  
675 Rasmussen et al. (202019)] at the top. The LA-ICPMS-based MDA's ages are also older than a  
676 ~216.6 Ma MDA determined on LA-ICPMS ages from an outcrop sample of sandstone in the  
677 middle part of the lower Sonsela Member, exposed ~132 km north of the CPCP core site (Marsh  
678 et al., 2019).

### 679 **8.6 Upper part of the Sonsela Member**

680 The lower five samples from the upper Sonsela Member yield similar preferred MDA's of  
681  $214.36 \pm 0.68$   $215.4 \pm 1.1/2.2$  Ma (sample 195-2),  $216.32 \pm 0.72$   $216.5 \pm 0.7/1.9$  Ma (sample 188-2),  
682  $216.19 \pm 0.62$   $216.1 \pm 0.9/2.1$  Ma (sample 182-1),  $214.81 \pm 0.70$   $215.1 \pm 0.8/1.9$  Ma (sample 177-1),  
683 and  $217.07 \pm 0.86$   $216.6 \pm 1.0/2.0$  Ma (sample 169-1). An upper sample yields a younger MDA of  
684  $214.18 \pm 0.54$   $213.8 \pm 0.6/2.1$  Ma (sample 158-2). All samples yield MSWD values greater than 1.0  
685 (average of 2.6) (DR Table 6), demonstrating the presence of multiple age components. Most  
686 samples have patterns of U concentration that suggest the possibility of Pb loss. The lower five  
687 MDA's are 2-3 m.y. older than CA-TIMS ages from equivalent strata, which include outcrop ages  
688 of ~213.9 (Ramezani et al., 2011), ~213.6 Ma (Nordt et al., 2015), and ~213.1 Ma (Ramezani et  
689 al., 2011), and CPCP core ages of ~214.0 Ma [samples 182-1 and 177-1; Rasmussen et al.  
690 (202019)]. A CA-TIMS age of ~213.5 Ma for the upper sample [158-2; Rasmussen et al.  
691 (202019)] is nearly identical to our age determination.

### 692 **8.7 Petrified Forest Member**

693 Our seven samples from the Petrified Forest Member yield three sets of preferred MDA's. The  
694 lowest unit (sample 131-2) yields an MDA of  $221.54 \pm 0.44$   $221.5 \pm 0.6/2.1$  Ma, which is  
695 significantly older than MDA's in adjacent strata. Four samples near the middle of the unit yield  
696 similar preferred MDA's of  $211.53 \pm 3.26$   $211.5 \pm 3.1/3.4$  Ma (sample 116-1),  $209.90 \pm 1.56$   $211.6 \pm$   
697  $1.7/2.5$  Ma (sample 104-3),  $210.42 \pm 1.08$   $211.2 \pm 1.2/1.9$  Ma (sample 92-2), and  
698  $211.86 \pm 0.94$   $211.7 \pm 1.0/2.0$  Ma (sample 84-2). These MDA's for two of these four samples  
699 overlap with are very similar to an ID-TIMS age of ~211.9 Ma (Irmis et al., 2011) from equivalent  
700 strata in outcrop, the other two younger MDA's may be compromised by Pb loss (Fig. 13).

701 Two upper samples, from the Black Forest bed, yield preferred MDA's of  $208.26 \pm 3.38$   $209.6 \pm$   
702  $3.0/3.4$  Ma (sample 66-1) and  $209.75 \pm 0.42$   $209.8 \pm 0.5/1.6$  Ma (sample 52-2). These MDA's are  
703 similar to CA-TIMS ages of ~210.2 Ma from core [sample 52-2; Rasmussen et al. (202019)] and



704 ~209.9 Ma from outcrop (Ramezani et al., 2011), but are significantly younger than outcrop-  
705 based ID-TIMS ages of ~211.0 Ma (Heckert et al., 2009) and ~213.0 Ma (Riggs et al., 2003). Most  
706 of our samples yield MSWD values greater than 1.0 (average of 1.5), suggesting the presence of  
707 multiple age components, and have patterns of U concentration that suggest the presence of  
708 Pb loss.

## 709 9. COMPARISON OF LA-ICPMS, CA-TIMS, AND MAGNETOSTRATIGRAPHIC CONSTRAINTS ON 710 DEPOSITIONAL AGE OF CHINLE FORMATION STRATA

711 ~~Our preferred maximum depositional ages for strata of the Chinle Formation range from ~223.3~~  
712 ~~to ~209.6 Ma, which is similar to the ~227.6 to ~209.9 Ma range of CA-TIMS ages (Fig. 13). All~~  
713 ~~available U-Pb data therefore suggest that the analyzed Chinle Formation strata are Late~~  
714 ~~Triassic, and probably Norian in age (Dickinson, 2018), given the assigned ages of ~237 to~~  
715 ~~~201.3 for Late Triassic time (Cohen et al., 2013) and ~227 to ~208.5 Ma (Cohen et al., 2013) or~~  
716 ~~~205.7 Ma (Kent et al., 2017) for Norian time.~~

717 ~~Figure 13 presents a comparison of our preferred maximum depositional ages, all available ID-~~  
718 ~~and CA-TIMS ages [from Riggs et al. (2003), Heckert et al. (2009), Ramezani et al. (2011), Irmis~~  
719 ~~et al. (2011), Atchley et al. (2013), Nordt et al., (2015), Kent et al. (2018), and Rasmussen et al.~~  
720 ~~(2019)], and two age models that are based on magnetostratigraphic and CA-TIMS~~  
721 ~~geochronologic information (Kent et al., 2019; Rasmussen et al., 2019). As shown on this figure,~~  
722 ~~our LA-ICPMS MDA's overlap with most CA-TIMS ages and both age models for most strata~~  
723 ~~belonging to the Blue Mesa Member and Petrified Forest Member, but are significantly older~~  
724 ~~for strata of the Sonsela Member. The following discussion explores this pattern of~~  
725 ~~convergence/divergence of the three chronometers—details of the magnetostratigraphic~~  
726 ~~information, CA-TIMS data, and age models are discussed by Kent et al. (2018, 2019) and~~  
727 ~~Rasmussen et al. (2019).~~

728 ~~Our preferred interpretation of the chronostratigraphic patterns is that U-Pb ages agree with~~  
729 ~~magnetostratigraphic ages for strata containing abundant zircon crystals which are air-fall in~~  
730 ~~origin, whereas U-Pb ages tend to predate deposition for strata that are dominated by zircon~~  
731 ~~grains recycled from older units. The difference in proportion of air-fall (near-depositional-age)~~  
732 ~~versus recycled (older) ages is interpreted to be controlled mainly by the grain size of the~~  
733 ~~sedimentary host, which is important because only >60  $\mu\text{m}$  zircon grains were analyzed in this~~  
734 ~~study. Given that most detrital zircon grains transported with mud and silt are less than 60  $\mu\text{m}$~~   
735 ~~in diameter, zircon grains analyzed from mudstone-siltstone samples (and sequences) are~~  
736 ~~interpreted to be dominated by air-fall crystals rather than older recycled components. In~~  
737 ~~contrast, because coarser grained sediment is able to transport >60  $\mu\text{m}$  zircon grains,~~  
738 ~~sandstone samples (and sequences) contain abundant recycled (older) zircon grains and a lower~~  
739 ~~proportion of air-fall (near-depositional-age) zircon grains.~~

740 ~~Our LA-ICPMS ages from sandstones are significantly impacted by this difference because zircon~~  
741 ~~grains were selected for analysis at random in an effort to generate an unbiased age~~

742 ~~distribution. CA-TIMS analyses from Chinle Formation sandstones have a higher yield of syn-~~  
743 ~~depositional ages because zircon grains were selected for analysis on the basis of their juvenile~~  
744 ~~appearance [e.g., acicular and prismatic crystals; Ramezani et al. (2011)] or from the youngest~~  
745 ~~grains in an LA-ICPMS data set (e.g., Rasmussen et al., 2019; Appendix 2).~~

746 ~~These interpreted connections between stratigraphy, grain size, and proportions of air-fall~~  
747 ~~versus recycled zircon grains lead to the interpretation that the three chronometric records~~  
748 ~~agree (to within ~1 m.y.) for strata of the lower Blue Mesa Member and middle-upper Petrified~~  
749 ~~Forest Member because these units are dominated by mudstone and siltstone, resulting in U-~~  
750 ~~Pb ages mainly from air-fall (or slightly reworked) zircon grains. In contrast, LA-ICPMS ages from~~  
751 ~~the Sonsela Member significantly pre-date deposition because the dominant sandstones~~  
752 ~~contain abundant zircon grains recycled from slightly older units. For strata of the upper~~  
753 ~~Sonsela Member, CA-TIMS ages approximate the true depositional age because the methods of~~  
754 ~~grain selection were successful in identifying populations of air-fall zircon grains. For strata of~~  
755 ~~the lower Sonsela Member, however, these methods were unsuccessful in identifying a~~  
756 ~~sufficient number of air-fall zircon grains to determine a reliable depositional age, presumably~~  
757 ~~because of their low abundance relative to recycled grains.~~

758 Our ~~preferred~~ maximum depositional ages for strata of the Chinle Formation range from  
759 ~223.213 to ~208.39.76 Ma, which is similar to the ~227.6 to ~209.9 Ma range of CA-TIMS ages  
760 (Fig. 13). All available U-Pb data therefore suggest that the analyzed Chinle Formation strata are  
761 Late Triassic, and probably Norian in age (Dickinson, 2018), given the assigned ages of ~237 to  
762 ~201.3 for Late Triassic time (Cohen et al., 2013) and ~227 to ~208.5 Ma (Cohen et al., 2013) or  
763 ~205.7 Ma (Kent et al., 2017) for Norian time.

764 Figure 13 presents a comparison of our LA-ICPMS-based average ages and preferred maximum  
765 depositional ages, all available ID- and CA-TIMS ages [from Riggs et al. (2003), Heckert et al.  
766 (2009), Ramezani et al. (2011), Irmis et al. (2011), Atchley et al. (2013), Nordt et al., (2015), Kent  
767 et al. (2018), and Rasmussen et al. (2020)], and two age models that are based on  
768 magnetostratigraphic and CA-TIMS geochronologic information (Kent et al., 2019; Rasmussen et  
769 al., 2020). As shown on this figure, our LA-ICPMS ages-MDA's reveal two first-order patterns.  
770 The first pattern is that the LA-ICPMS-based ages-MDA's overlap with most CA-TIMS ages and  
771 both age models for most strata belonging to the Blue Mesa Member and Petrified Forest  
772 Member, but are significantly older for strata of the Sonsela Member. The second pattern is  
773 that most LA-ICPMS-based ages-MDA's belong to five main clusters (~223 Ma, ~222-220 Ma,  
774 ~217-215 Ma, ~212-211, and ~210 Ma), whereas the other chronologic records show a  
775 relatively simple pattern of upward younging (Fig. 13). The following discussion explores these  
776 two patterns – details of the magnetostratigraphic information, CA-TIMS data, and age models  
777 are discussed by Kent et al. (2018, 2019) and Rasmussen et al. (2020).

778 As shown on Figure 13, the LA-ICPMS-based average ages and MDA's presented herein overlap  
779 with the other chronometers for sequences which are dominated by fine-grained strata (e.g.,  
780 Blue Mesa Member and Petrified Forest Member), but are several million years too old for

781 sequences which are dominated by coarse-grained strata (Sonsela Member) (Fig. 13). This  
782 pattern appears to hold for member-scale stratigraphic units (e.g., strata from the Petrified  
783 Forest Member), although some individual samples clearly do not follow this pattern. For  
784 example, of the six samples from the Petrified Forest Member that yield LA-ICPMS  
785 ~~ages~~maximum depositional ages which overlap with the other chronometers, four are  
786 mudstone-siltstone and two are sandstone. In the lower Sonsela Member, of the six samples  
787 ~~with that LA-ICPMS ages~~yield maximum depositional ages that predate the other  
788 chronometers, five are sandstone and one is siltstone. These exceptions suggest that the  
789 dominant lithic characteristics and depositional environment of a member (e.g., dominantly  
790 fine-grained floodplain deposits for the Petrified Forest Member versus dominantly coarse-  
791 grained channel deposits of the Sonsela Member [Woody, 2006]), are more important than the  
792 grain size of an individual horizon in controlling the recognition of near-depositional-age zircon  
793 grains.

794 The observed pattern that predominantly fine-grained strata of the Mesa Redondo, Blue Mesa,  
795 and Petrified Forest members yield reliable LA-ICPMS ages~~MDA's~~, whereas predominantly  
796 coarse-grained sandstones of the Sonsela Member do not, is surprising for two reasons. First, in  
797 terms of provenance (as described above), strata of the Mesa Redondo, Blue Mesa, and  
798 Petrified Forest members are interpreted to have been shed mainly from the Ouachita orogen,  
799 which lacks Triassic igneous rocks, whereas strata of the Sonsela Member were shed from the  
800 Cordilleran magmatic arc to the southwest, which contains abundant Permian and Triassic  
801 igneous rocks (Fig. 3). Second, as shown in the margins of Figures 7 and 8, Triassic zircon grains  
802 are significantly (~2x) more abundant in strata of the Sonsela Member than in underlying and  
803 overlying strata. Based on these two observations, one might expect that strata of the Sonsela  
804 Member would yield reliable MDA's, whereas strata from the Mesa Redondo Member, Blue  
805 Mesa Member, and Petrified Forest Member would not.

806 We suggest that these counter-intuitive relations result in large part from our analytical method  
807 of only analyzing zircon grains that are >60 um, combined with the maximum size of zircons  
808 that can be transported in fine-grained versus coarse-grained sediments. For coarse-grained  
809 sediment, >60 um zircon grains could include both transported (detrital) components that  
810 predate deposition, as well as zircons that are air-fall in origin and approximately of  
811 depositional age. A MDA calculated from a mix of these grains would accordingly pre-date  
812 deposition. In contrast, Triassic zircon grains from fine-grained strata would tend to be mostly  
813 air-fall in origin given that the older, transported grains are too small to analyze. An MDA  
814 calculated from zircons that are primarily of air-fall origin would accordingly approach the true  
815 depositional age.

816 The relations described above suggest that convergence versus divergence of the chronologic  
817 records results from connections between depositional setting, grain size, provenance, and  
818 analytical methods, which together conspire to control the proportions of air-fall (near-  
819 depositional age) versus slightly older detrital zircon grains recognized in our samples. We

820 suggest that the three chronometric records agree (to within  $\sim 1-2$  m.y.) for strata of the lower  
821 Blue Mesa Member and middle-upper Petrified Forest Member because of the availability of  
822 zircon grains of air-fall origin, which are near depositional age and both  $<60$   $\mu\text{m}$  and  $>60$   $\mu\text{m}$  in  
823 size, versus the scarcity of pre-depositional-age Triassic grains of sufficient size for analysis due  
824 to the lack of Triassic rocks in the source region (mainly the Ouachita orogen) and the small  
825 ( $<60$   $\mu\text{m}$ ) grain size of most sediment. In contrast, for the Sonsela Member, the LA-ICPMS  
826 average ages and MDA's are interpreted to pre-date the other chronologic records because the  
827 sediment was derived from the south, where abundant igneous rocks of Permian-Triassic age  
828 were exposed, and the grain size of the detrital (pre-depositional-age) zircons was sufficiently  
829 large that many would have been analyzed.

830 A test of this hypothesis is provided by MSWD values of the weighted means calculated for ages  
831 from samples belonging to the various stratigraphic units. As shown in DR Table 6, average  
832 MSWD values for samples from dominantly fine-grained strata of the Mesa Redondo-Blue Mesa  
833 and Petrified Forest units are 1.7 and 1.3 (respectively), whereas coarser grained strata of the  
834 lower and upper Sonsela units yield higher MSWD values of 2.6 and 2.1 (respectively). These  
835 values are consistent with the interpretation that Triassic zircon grains in coarser-grained units  
836 have a greater range of ages than Triassic zircon grains in finer-grained units.

837 These interpreted connections may also provide an explanation for the patterns of offset of the  
838 CA-TIMS ages of Rasmussen et al. (2020) relative to the LA-ICPMS ages and  
839 magnetostratigraphic age models in the Sonsela Member (Fig. 13). For strata of the upper  
840 Sonsela Member, the CA-TIMS and magnetostratigraphic records converge because the  
841 methods of grain selection were apparently successful in identifying populations of syn-  
842 depositional age zircon grains. For strata of the lower Sonsela Member, however, these  
843 methods were unsuccessful in identifying a sufficient number of depositional-age zircon grains  
844 to determine a reliable MDA, presumably because of their low abundance relative to older  
845 transported grains.

846 The second main pattern exhibited by the three chronometers is that most of the LA-ICPMS-  
847 based average ages and MDA's belong to ~~five~~<sup>three</sup> main clusters ( $\sim 223$  Ma,  $\sim 222-220$  Ma,  $\sim 217-$   
848  $215$  Ma, ~~and~~  $\sim 212-211$ , and  $\sim 210$  Ma), whereas the other chronologic records show a relatively  
849 simple pattern of upward younging (Fig. 13). For the  $\sim 222-220$  Ma cluster, a plausible  
850 interpretation, following from the connections described above, is that  $\sim 222-220$  Ma zircon  
851 grains of air-fall origin accumulated in fine-grained strata of the lower Blue Mesa Member, and  
852 were then recycled from age-equivalent strata into predominantly coarser grained channel  
853 sands of the upper Blue Mesa Member and lower Sonsela Member. Grains from these same  
854 sources appear to have also been recycled into sandstone sample 131-2 of the lower Petrified  
855 Forest Member (Fig. 13). The  $\sim 212-211$  Ma cluster may have formed in a similar fashion, with  
856 initial accumulation of near-depositional-age air-fall zircons in mudstones of sample 116-1,  
857 followed by recycling of these grains from age-equivalent strata into coarser-grained strata of  
858 samples 104-3, 92-2, and 84-2 (Fig. 13).

859 The source of zircon grains that belong to the ~217-215 Ma cluster is less obvious given the lack  
860 of recognized fine-grained strata dominated by zircons of this age (Fig. 13). One possibility is  
861 that ~217-215 Ma grains were eroded from fine-grained strata exposed elsewhere [perhaps  
862 near Sonsela Buttes (Marsh et al., 2019) or near the Cordilleran magmatic arc] that are  
863 dominated by grains of this age. A second possibility is that fine-grained strata dominated by  
864 ~217-215 Ma ages were originally present in the lower Sonsela Member, but were removed by  
865 erosion and recycled into strata of the upper Sonsela Member. Previous workers have  
866 suggested the existence of a hiatus or hiatuses (Ramezani et al., 2011) or an erosional event  
867 (Rasmussen et al., 2020) at approximately this stratigraphic level, as shown by the preferred  
868 age model of Rasmussen et al. (2020) on Figure 13. The occurrence of very different <240 Ma  
869 ages, >240 Ma ages, and U/Th values in samples 196-3 and 195-2 suggests that this shift in  
870 provenance, accumulation of a condensed section, or formation of an unconformity likely  
871 coincides with the proposed boundary between strata of the lower Sonsela Member and upper  
872 Sonsela Member. As discussed by Ramezani et al. (2011) and Rasmussen et al. (2020), the  
873 possibility of an unconformity or condensed section near this stratigraphic position has  
874 important implications for Chinle stratigraphy and fundamental Late Triassic biotic and climatic  
875 changes. It should be noted, however, that no stratigraphic evidence for such an unconformity  
876 was recognized in the CPCP core.

## 877 **10. IMPLICATIONS FOR THE STRATIGRAPHY OF THE CHINLE FORMATION**

878 The interpreted connections between the three geochronologic records and Chinle stratigraphy  
879 provide an opportunity to reconstruct the depositional history of the Chinle Formation.  
880 Fundamental assumptions in reconstructing this history are that:

881 (1) Chinle Formation strata encountered in the CPCP core record nearly continuous deposition  
882 as described in the age model of Kent et al. (2019), perhaps with a period of erosion or very  
883 slow deposition in the middle part of the Sonsela Member (Rasmussen et al., [2019/2020](#)).

884 (2) LA-ICPMS ages recovered from strata of the Chinle Formation belong to five separate groups  
885 (red vertical bars of Figure 13) due to the hypothesized connections between stratigraphy, grain  
886 size, and proportions of near-depositional-age (air-fall) versus older (recycled) zircon ages.

887 (3) Late Triassic igneous activity in the Cordilleran magmatic arc provided a nearly continuous  
888 supply of zircon grains of air-fall origin to the Chinle deposystem. This assumption is supported  
889 by the relatively continuous distribution of U-Pb ages within the Cordilleran magmatic arc and  
890 back-arc (upper curves of Figure 13). ~~This view is in contrast to the hypothesis of Kent et al.  
891 (2019) that variations in the proportions of depositional-age versus older zircon grains result  
892 mainly from temporal changes in magmatic flux.~~

893 The interpreted stratigraphic evolution is summarized below and shown schematically on  
894 Figure 14. Important phases in this evolution are as follows:

895 A: An LA-ICPMS MDA of ~223.3 Ma from our one sample from the Mesa Redondo Member  
896 (305-2) agrees with the magnetostratigraphic information, the two age models, and the set of  
897 CA-TIMS ages from this sample, presumably because these fine-grained strata are dominated  
898 by zircon grains of air-fall origin. Older CA-TIMS ages of ~225.2 Ma (Ramezani et al., 2011) and  
899 ~227.6 (Atchley et al., 2013) from outcrops of the Mesa Redondo Member may be  
900 compromised by an abundance of recycled zircon grains.

901 B: LA-ICPMS average ages of ~221-220 Ma for most grains from fine-grained strata in the lower  
902 part of the Blue Mesa Member are also near depositional age, presumably because the >60 um  
903 zircon grains in these fine-grained strata are dominated by air-fall (or slightly reworked)  
904 components. Minimum ages for these samples are somewhat younger, presumably due to Pb  
905 loss.

906 C: LA-ICPMS ages from strata of the upper Blue Mesa Member significantly pre-date deposition,  
907 presumably because these strata are dominated by recycled zircons. The predominance of  
908 ~221-220 Ma LA-ICPMS MDA's ages suggests that most zircon grains were recycled from lateral  
909 equivalents of underlying strata in the lower part of the Blue Mesa Member. CA-TIMS ages also  
910 pre-date deposition, presumably because of the difficulty of isolating near-depositional-age  
911 grains of air-fall origin.

912 D: This pattern continues up through most of the lower Sonsela Member, with LA-ICPMS  
913 agesMDA's remaining at ~221-220 Ma (except where compromised by Pb loss) due to recycling  
914 of strata from lateral equivalents of the lower Blue Mesa Member. Most CA-TIMS ages predate  
915 the age of deposition because depositional-age (air fall) grains were diluted by recycled  
916 components.

917 E: The age patterns from sandstones of the upper Sonsela Member are somewhat puzzling  
918 given that the dominant ~217-215 Ma LA-ICPMS ages MDA's pre-date deposition, but fine-  
919 grained strata that could have sourced grains of these ages are not present in the lower Sonsela  
920 Member (Fig. 13). One possibility, as described above, is that the ~217-215 Ma grains were  
921 eroded from fine-grained strata exposed elsewhere [~~perhaps near Sonsela Buttes~~ (Marsh et  
922 al., 2019) or from the Cordilleran magmatic arc] that are dominated by grains of this age. A  
923 second possibility is that fine-grained strata dominated by ~217-215 Ma ages were originally  
924 present in the underlying lower Sonsela Member, but were removed by erosion and recycled  
925 into strata of the upper Sonsela Member. An erosional event of the appropriate age and  
926 stratigraphic position has been described by Ramezani et al. (2011) and by Rasmussen et al.  
927 (202019), as shown by their age model on Figure 13. The occurrence of very different <240 Ma  
928 ages, >240 Ma ages, and U/Th values in samples 196-3 and 195-2 suggests that this change in  
929 provenance, condensed section, or unconformity most likely coincides with the boundary  
930 between lower and upper Sonsela Member strata, ~~and perhaps with the red siliceous horizon~~  
931 ~~recognized in the CPCP core.~~ As discussed by Rasmussen et al. (202019), the possibility of an  
932 unconformity or condensed section near this stratigraphic position has important implications  
933 for Chinle stratigraphy and fundamental Late Triassic biotic and climatic changes.

934 F: The dominance of pre-depositional-age grains in sample 131-2 provides strong evidence for  
935 recycling of detrital zircons from lateral equivalents of underlying strata of the Blue Mesa  
936 Member or lower Sonsela Member.

937 G: All chronometers agree for strata of sample 116-1, presumably because these fine-grained  
938 strata are dominated by air-fall (or slightly reworked) detrital zircons.

939 H: LA-ICPMS ages MDA's from sandstones of the middle Petrified Forest Member (samples 104-  
940 3, 92-2, and 84-2) slightly predate deposition (except where compromised by Pb loss) because  
941 they were recycled from lateral equivalents of immediately underlying fine-grained strata (e.g.,  
942 sample 116-1).

943 I: Most LA-ICPMS ages agree with the other All-chronometers agree for strata of the Black  
944 Forest bed because this unit is dominated by air-fall (or slightly reworked) detrital zircon grains.  
945 The minimum age for sample 66-1 is somewhat younger, presumably due to Pb loss.

## 946 **11. CONCLUSIONS**

947 First-order conclusions that result from our U-Pb geochronologic analyses of detrital zircon  
948 grains from the Coconino Sandstone, Moenkopi Formation, and Chinle Formation are as  
949 follows:

950 1. The provenance of strata belonging to the Coconino Sandstone and Moenkopi Formation can  
951 be reconstructed by comparison of our LA-ICPMS ages (Figures 5 and 6) with age distributions  
952 that characterize potential source regions (Figure 3). As shown on Figures 5 and 11, data from  
953 our sample of the Coconino Sandstone and equivalent sandstones of the southern Colorado  
954 Plateau suggest that these strata belong to an eolian blanket that was derived largely from the  
955 Ouachita and/or Appalachian orogens, whereas strata from the northern Colorado Plateau  
956 consist mainly of sediment derived from local basement uplifts (Fig. 1; Dickinson and Gehrels,  
957 2003; Gehrels et al., 2011; Lawton et al., 2015). Lower-Middle Triassic strata of the Moenkopi  
958 Formation record a very different dispersal system, with most detritus derived from the  
959 Ouachita orogen, the East Mexico arc, and early phases of the Cordilleran magmatic arc (Figures  
960 6 and 9).

961 2. LA-ICPMS ages from strata of the Chinle Formation belong to five groups that generally  
962 correspond to the main stratigraphic units (Figures 7, 8, and 13). Maximum depositional ages  
963 calculated from <240 Ma ages and provenance interpretations derived from >240 Ma ages are  
964 as follows:

965 -- Strata of the Mesa Redondo Member yield a preferred MDA of ~223.3 Ma, and were derived  
966 mainly from the Ouachita orogen.

967 -- Strata of the Blue Mesa Member yield MDA's of ~221.20.7 to ~218.620.2 Ma, and were  
968 derived from local basement and Ouachita sources.

969 -- Strata in the lower part of the Sonsela Member yield similar MDA's of  $\sim 221.30.9$  to  
970  $\sim 219.220.3$  Ma (plus an uppermost sample with an MDA of  $\sim 217.98.2$  Ma). Detritus was derived  
971 mainly from local basement (especially  $\sim 1.44$  Ga) sources, perhaps located in the ancestral  
972 Mogollon highlands to the south.

973 -- Strata in the upper part of the Sonsela Member yield younger MDA's of  $\sim 217.16.6$  to  
974  $\sim 214.45.1$  Ma, plus an uppermost sample with an MDA of  $\sim 214.23.8$  Ma. Grains with  $>240$  Ma  
975 ages were derived mainly from Precambrian basement (mainly  $\sim 1.44$  Ga) and Grenville-age  
976 rocks to south, as well as the East Mexico arc.

977 -- Strata of the Petrified Forest Member yield LA-ICPMS ages that belong to three separate  
978 groups. The lowest sample yields an MDA of  $\sim 221.5$ , which is significantly older than ages from  
979 adjacent strata. The middle four samples yield MDA's of  $\sim 211.97$  to  $\sim 209.944.2$  Ma, whereas  
980 the upper two samples yield MDA's of  $\sim 209.8$  and  $\sim 208.39.6$  Ma. All six upper samples contain  
981 abundant  $>240$  Ma grains that were shed from a broad range of Ouachita, local basement, and  
982 East Mexico arc sources.

983 3. Patterns of U and Th concentration in Triassic zircon grains from the Chinle Formation belong  
984 to four distinct groups that generally coincide with the chronostratigraphic units described  
985 above. Changes in U and Th concentrations are interpreted to record variations in the chemistry  
986 of arc magmatism through time, as has been documented previously by Barth and Wooden  
987 (2006, 2011, 2013) and Riggs et al. (2010, 2012, 2016).

988 4. Comparison of the Chinle Formation MDA's with magnetostratigraphic information (Kent et  
989 al., 2018, 2019) and CA-TIMS geochronologic information (Rasmussen et al., 202019) from the  
990 CPCP core, plus CA-TIMS ages reported from outcrop samples, indicates that LA-ICPMS MDA's  
991 approximate depositional ages for most strata of the Mesa Redondo Member, Blue Mesa  
992 Member, and Petrified Forest Member (except where compromised by Pb loss), but  
993 significantly pre-date deposition for strata of the Sonsela Member (Fig. 13). The correlation of  
994 age patterns with stratigraphy is interpreted to reflect the proportions of air-fall (or slightly  
995 reworked) versus recycled (older) zircon grains: fine-grained strata are dominated by near-  
996 depositional ages because most zircon grains are air-fall (or slightly reworked) in origin,  
997 whereas coarse-grained strata are dominated by pre-depositional ages because recycled zircon  
998 grains dilute the abundance of air-fall crystals.

999 5. This hypothesized connection between stratigraphy and the three geochronologic records  
1000 supports the following depositional history for Chinle Formation strata encountered in the CPCP  
1001 core (Figures 13 and 14):

1002 -- LA-ICPMS ages and magnetostratigraphic information (Kent et al., 2019) indicate that the  
1003 sampled part of the Mesa Redondo Formation was deposited at  $\sim 223.3$  Ma. CA-TIMS ages of  
1004  $\sim 225.2$  Ma (Ramezani et al., 2011) and  $\sim 227.6$  (Atchley et al., 2013) from outcrop samples  
1005 suggest that strata of the Mesa Redondo Member in other areas are dominated by older  
1006 recycled components.



1007 -- Magnetostratigraphic information (Kent et al., 2019) suggests that strata of the Blue Mesa  
1008 Member and lower Sonsela Member accumulated between ~222 Ma and ~214 Ma, whereas  
1009 LA-ICPMS MDA's are consistently ~~~222-220~~ Ma for the same strata (except for the uppermost  
1010 sample of ~~~217-218~~ Ma). This suggests that most zircons in strata of the upper Blue Mesa  
1011 Member and lower Sonsela Member were recycled from lateral equivalents of strata of the  
1012 lower Blue Mesa Member. The observation that most CA-TIMS ages from these strata also pre-  
1013 date deposition is interpreted to result from the dilution of air-fall zircon crystals by older  
1014 recycled zircon grains.

1015 -- Strata of the upper Sonsela Member accumulated between ~215 and ~213 Ma, as  
1016 constrained by magnetostratigraphic information and CA-TIMS ages. LA-ICPMS MDAs from  
1017 these strata are ~217-215 Ma, which indicates that they are dominated by zircons recycled  
1018 from older units. The lack of samples in the lower Sonsela Member that are dominated by  
1019 ~217-215 Ma grains suggests that zircon grains of this age in upper Sonsela Member strata may  
1020 have been transported from sections of the Chinle Formation exposed outside of the PEFO  
1021 area. It is also possible that such strata were exposed in the PEFO area, but were removed  
1022 during an erosional event inferred by Rasmussen et al. (20~~2019~~) from the pattern of CA-TIMS  
1023 ages in the upper Sonsela Member (Fig. 3). Significant changes in <240 Ma ages, >240 Ma ages,  
1024 and U-Th values suggest that this unconformity, if present, occurs between samples 196-3 and  
1025 195-2, ~~and may coincide with the red siliceous horizon recognized in the CPCP core.~~

1026 -- All available evidence suggests that mudstone and subordinate sandstone of the middle  
1027 Petrified Forest Member accumulated at ~212-211 Ma, and the Black Forest bed in the upper  
1028 part of the unit accumulated at ~210 Ma. In contrast, LA-ICPMS ages recovered from sample  
1029 131-2, from the lower part of the Petrified Forest Member, are dominantly ~221 Ma, suggestive  
1030 of recycling from lateral equivalents of strata of the Blue Mesa Member and lower Sonsela  
1031 Member.

1032 6. Comparisons of our LA-ICPMS ages, the available CA-TIMS data, and magnetostratigraphic  
1033 information provide insights into methods for determining the depositional age of fluvial strata.  
1034 Our results show that the most reliable information comes from sequences dominated by fine-  
1035 grained clastic strata (mudstone and siltstone) given that these strata have a low abundance of  
1036 pre-depositional-age zircon grains of the appropriate size (>60  $\mu\text{m}$  diameter) for routine  
1037 analysis by LA-ICPMS. Mudstone-siltstone samples may accordingly ~~yield have~~ a high proportion  
1038 of >60  $\mu\text{m}$  zircon grains that are air-fall in origin (or only slightly reworked) and thereby record  
1039 the age of deposition. In contrast, sedimentary sequences dominated by sandstone could well  
1040 commonly yield abundant >60  $\mu\text{m}$  zircon grains that predate deposition ~~have been recycled~~  
1041 ~~from older sediments~~, thereby diluting syn-depositional-age zircon grains. Future attempts to  
1042 determine depositional ages from fluvial strata should accordingly focus on sequences  
1043 dominated by fine-grained strata, rather than sandstones, in spite of the challenges of  
1044 extracting and analyzing the smaller zircon crystals.

## 1045 12. CODE/DATA AVAILABILITY

1046 [All data are available from the included supplementary tables.](#)

### 1047 **13. AUTHOR CONTRIBUTION**

1048 [NG and GG generated the LA-ICPMS data reported in this paper. All coauthors were involved in](#)  
1049 [acquiring the samples that were analyzed and/or interpreting the data. GG prepared this](#)  
1050 [manuscript with input from all co-authors.](#)

### 1051 **14. COMPETING INTERESTS**

1052 [The authors declare that they have no conflict of interest.](#)

### 1053 ~~**12. AUTHOR CONTRIBUTION**~~

1054 ~~[NG and GG generated the LA-ICPMS data reported in this paper. All coauthors were involved in](#)~~  
1055 ~~[acquiring the samples that were analyzed and/or interpreting the data. GG prepared this](#)~~  
1056 ~~[manuscript with input from all co-authors.](#)~~

### 1057 ~~**13. COMPETING INTERESTS**~~

1058 ~~[The authors declare that they have no conflict of interest.](#)~~

### 1059 **14. ACKNOWLEDGEMENTS**

1060 Geochronologic analyses were conducted with support from NSF EAR-0959107 and EAR-  
1061 1649254 (to Gehrels). Laboratory analyses were performed primarily by N. Giesler.  
1062 Collaborative aspects of the project were supported by NSF EAR 0958976 (PEO & JWG),  
1063 0958723 (RM), 0958915 (RBI), and 0958859 (DVK). Funding for coring and much logistical  
1064 support was provided by ICDP (International Scientific Continental Drilling Program grant 05-  
1065 2010: JWG, PEO, Jingeng Sha, Roberto Molina-Garza, Wolfram Kürschner, and Gerhard  
1066 Bachmann). Additional funding was supplied by grants from the Lamont Climate Center (PEO).  
1067 Field support was provided by LacCore personnel (Anders Noren, Kristina Brady, and Ryan  
1068 O'Grady), drilling manager Doug Schnurrenberger, and core-handling volunteers (Justin Clifton,  
1069 Bob Graves, Ed Lamb, Max Schnurrenberger, and Riley Black). Superintendent Brad Traver of  
1070 the National Park Service arranged for permission to core in the PEFO and provided logistical  
1071 support during site selection and drilling. This is Petrified Forest Paleontological Contribution 67.  
1072 The conclusions presented here are those of the authors and do not represent the views of the  
1073 United States Government.

1074 **REFERENCES CITED**

- 1075 Alsalem, O.B., Fan, M., Zamora, J., Xie, X., and Griffin, W.R.: Paleozoic sediment dispersal before  
1076 and during the collision between Laurentia and Gondwana in the Fort Worth Basin, USA:  
1077 *Geosphere*, v. 14, no. 1, p. 1–18, doi: 10.1130/GES01480.1, 2018.
- 1078 Ash, S.R.: The Black Forest Bed, a distinctive unit in the Upper Triassic Chinle Formation, north-  
1079 eastern Arizona: *Journal of the Arizona-Nevada Academy of Science*, v. 24–25, p. 59–73, 1992.
- 1080 Atchley, S.C., Nordt, L.C., Dworkin, S.I., Ramezani, J., Parker, W.G., Ash, S.R., and Bowring, S.A.:  
1081 A linkage among Pangean tectonism, cyclic alluviation, climate change, and biologic turnover in  
1082 the Late Triassic: The Record from the Chinle Formation, Southwestern United States: *Journal of*  
1083 *Sedimentary Research*, v. 83, p. 1147–1161, 2013.
- 1084 Baranyi, V., Reichgelt, T., Olsen, P.E., Parker, W.G., Kürschner, W.M.: Norian vegetation history  
1085 and related environmental changes: new data from the Chinle Formation, Petrified Forest  
1086 National Park (Arizona, SW USA): *Geological Society of America Bulletin*, v. 130, p. 775–795,  
1087 doi.org/10.1130/B31673.1, 2017.
- 1088 Barth, A.P. and Wooden, J.L.: Timing of magmatism following initial convergence at a passive  
1089 margin, southwestern US Cordillera, and ages of lower crustal magma sources: *Journal of*  
1090 *Geology*, v. 114, p. 231–245, 2006.
- 1091 Barth, A.P., Walker, J.D., Wooden, J.L., Riggs, N.R., and Schweickert, R.A.: Birth of the Sierra  
1092 Nevada magmatic arc: Early Mesozoic plutonism and volcanism in the east-central Sierra  
1093 Nevada of California: *Geosphere*, v. 7, p. 877–897, 2011.
- 1094 Barth, A.P., Wooden, J.L., Jacobson, C.E., and Economos, R.C.: Detrital zircon as a proxy for  
1095 tracking the magmatic arc system: The California arc example: *Geology*, v. 41, p. 223–226, 2013.
- 1096 Black, L., Kamo, S., Allen, C., Davis, D., Aleinikoff, J., Valley, J., Mundil, R., Campbell, I., Korsch,  
1097 R., Williams, I., and Foudoulis, C.: Improved  $^{206}\text{Pb}/^{238}\text{U}$  microprobe geochronology by the  
1098 monitoring of a trace-element-related matrix effect; SHRIMP, ID-TIMS, ELA-ICP-MS and  
1099 oxygen isotope documentation for a series of zircon standards: *Chemical Geology*, v. 205, p.  
1100 115–140, 2004.
- 1101 Blakey, R.C., Peterson, F., and Kocurek, G.: Synthesis of late Paleozoic and Mesozoic eolian  
1102 deposits of the western interior of the United States: *Sedimentary Geology*, v. 56, p. 3–125,  
1103 1988.
- 1104 Chen, J.H., and Moore, J.G.: Uranium-lead isotopic ages from the Sierra Nevada batholith:  
1105 *Journal of Geophysical Research*, v. 87, p. 4761–4784, 1982.
- 1106 Cohen, K.M., Finney, S.C., Gibbard, P.L., and Fan, J.-X.: The ICS International Chronostratigraphic  
1107 Chart: Episodes v. 36, p. 199–204 (updated 2018), 2013.

1108 Creber, G.T., and Ash, S.R.: Evidence of widespread fungal attack on Upper Triassic trees in the  
1109 southwestern U.S.A.: *Review of Palaeobotany and Palynology*, v. 63, p. 189-195, 1990.

1110 DeGraaff-Surples, K., Graham, S.A., Wooden, J.L., and McWilliams, M.O.: Detrital zircon  
1111 provenance analysis of the Great Valley Group, California: Evolution of an arc-forearc system:  
1112 *Geological Society of America Bulletin*, v. 114 (12), p. 1564–1580, 2002.

1113 Dickinson, W.R.: Tectonosedimentary Relations of Pennsylvanian to Jurassic strata on the  
1114 Colorado Plateau, *Geological Society of America Special Paper 533*, 184 p., 2018.

1115 Dickinson, W.R., and Gehrels, G.E.: U-Pb ages of detrital zircon grains from Permian and Jurassic  
1116 eolian sandstones of the Colorado Plateau, USA: Paleogeographic implications: *Sedimentary  
1117 Geology*, v. 163, p. 29–66, 2003.

1118 Dickinson, W.R. and Gehrels, G.E.: U-Pb ages of detrital zircon grains in relation to  
1119 paleogeography: Triassic paleodrainage networks and sediment dispersal across southwest  
1120 Laurentia: *Journal of Sedimentary Research*, v. 78, p. 745–764, 2008.

1121 Dickinson, W.R. and Gehrels, G.E.: Use of U–Pb ages of detrital zircon grains to infer maximum  
1122 depositional ages of strata: a test against a Colorado Plateau Mesozoic database: *Earth and  
1123 Planetary Science Letters*, v. 288, p. 115–125, 2009.

1124 [Galbraith, R. and Laslett, G.: Statistical models for mixed fission track ages: Nuclear tracks and  
1125 radiation measurements, v. 21 \(4\), p. 459-470, 1993.](#)

1126 Gehrels, G.E.: Introduction to detrital zircon studies of Paleozoic and Triassic strata in western  
1127 Nevada and northern California, in Soreghan, M.J. and Gehrels, G.E., eds., *Paleozoic and Triassic  
1128 paleogeography and tectonics of western Nevada and northern California: Geological Society of  
1129 America Special Paper 347*, p. 1-18, 2000.

1130 Gehrels, G.E.: Detrital zircon U-Pb geochronology applied to tectonics: *Annual Review of Earth  
1131 and Planetary Sciences*, v. 42, p. 127-149, 2014.

1132 Gehrels, G. and Pecha, M.: Detrital zircon U-Pb geochronology and Hf isotope geochemistry of  
1133 Paleozoic and Triassic passive margin strata of western North America: *Geosphere*, v. 10 (1), p.  
1134 49-65, 2014.

1135 Gehrels, G.E., Valencia, V., Pullen, A.: Detrital zircon geochronology by Laser-Ablation  
1136 Multicollector ICPMS at the Arizona LaserChron Center, in Loszewski, T., and Huff, W., eds.,  
1137 *Geochronology: Emerging Opportunities, Paleontology Society Short Course: Paleontology  
1138 Society Papers*, v. 11, 10 p., 2006.

1139 Gehrels, G.E., Valencia, V., Ruiz, J.: Enhanced precision, accuracy, efficiency, and spatial  
1140 resolution of U-Pb ages by laser ablation–multicollector–inductively coupled plasma–mass  
1141 spectrometry: *Geochemistry, Geophysics, Geosystems*, v. 9, Q03017,  
1142 doi:10.1029/2007GC001805, 2008.

- 1143 Gehrels, G., Blakey, R., Karlstrom, K., Timmons, M., Dickinson, W., and Pecha, M.: Detrital zircon  
1144 U-Pb geochronology of Paleozoic strata in the Grand Canyon: *Lithosphere*, v. 3 (3), p. 183-200,  
1145 2011.
- 1146 González-León, C.M., Valencia, V.A., Lawton, T.F., Amato, J.M., Gehrels, G.E., Leggett, W.J.,  
1147 Montijo-Contreras, O., Fernández, M.A.: The lower Mesozoic record of detrital zircon U-Pb  
1148 geochronology of Sonora, México, and its paleogeographic implications: *Revista Mexicana de*  
1149 *Ciencias Geológicas*, v. 26 (2), p. 301-314, 2009.
- 1150 Heckert, A.B. and Lucas, S.G.: Revised Upper Triassic stratigraphy of the Petrified Forest  
1151 National Park, Arizona, USA: *New Mexico Museum of Natural History Science Bulletin*, v. 21, p.  
1152 1–36, 2002.
- 1153 Heckert, A.B., Lucas, S.G., Dickinson, W.R., and Mortensen, J.K.: New ID-TIMS U-Pb ages for  
1154 Chinle Group strata (Upper Triassic) in New Mexico and Arizona, correlation to the Newark  
1155 Supergroup, and implications for the “long Norian”: *Geological Society of America Abstracts*  
1156 *with Programs*, v. 41, p. 123, 2009.
- 1157 Hildebrand, R.S.: Did westward subduction cause Cretaceous-Tertiary orogeny in the North  
1158 American Cordillera?: *Geological Society of America Special paper* 457, 71 p., 2009.
- 1159 Hildebrand, R.S.: Mesozoic assembly of the North American cordillera: *Geological Society of*  
1160 *America Special paper* 495, 169 p., 2013.
- 1161 Hoke, G., Schmitz, M., and Bowring, S.: An ultrasonic method for isolating nonclay components  
1162 from clay-rich material: *Geochemistry Geophysics Geosystems*, v. 15, p. 492–498, 2014.
- 1163 Horstwood, M., Kosler, J., Gehrels, G., Jackson, S., McLean, N., Paton, C., Pearson, N., Sircombe,  
1164 K., Sylvester, P., Vermeesch, P., Bowring, J., Condon, D., and Schoene, B.: Community-Derived  
1165 Standards for LA-ICP-MS U-Th-Pb Geochronology – Uncertainty Propagation, Age Interpretation  
1166 and Data Reporting: *Geostandards and Geoanalytical Research*, v. 40 (3), p. 311-332, 2016.
- 1167 Irmis, R.B., Mundil, R., Martz, J.W., and Parker, W.G.: High-resolution U-Pb ages from the Upper  
1168 Triassic Chinle Formation (New Mexico, USA) support a diachronous rise of dinosaurs: *Earth and*  
1169 *Planetary Science Letters*, v. 309, p. 258–267, 2011.
- 1170 Kent, D.V., Olsen, P.E., and Muttoni, G.: Astrochronostratigraphic polarity time scale (APTS) for  
1171 the Late Triassic and Early Jurassic from continental sediments and correlation with standard  
1172 marine stages: *Earth-Science Reviews*, v. 166, p. 153–180, 2017.
- 1173 Kent, D.V., Olsen, P.E., Rasmussen, C., Lepre, C.J., Mundil, R., Irmis, R.B., Gehrels, G.E., Giesler,  
1174 D., Geissman, J.W., and Parker, W.G.: Empirical evidence for stability of the 405 kyr Jupiter-  
1175 Venus eccentricity cycle over hundreds of millions of years: *Proceedings of the National*  
1176 *Academy of Sciences*, v. 115, p. 6153–6158, 2018.

1177 Kent, D.V., Olsen, P.E., Lepre, C. Mundil, R., Rasmussen, C., Irmis, R.B., Gehrels, G.E., Giesler, D.,  
1178 Geissman, J.W., Parker, W.G.: Magnetostratigraphy of the entire Chinle Formation (Norian age)  
1179 in scientific drill core PFNP-1A from the Petrified Forest National Park (Arizona, USA) and  
1180 implications for global correlations in the Late Triassic: *Geophysics, Geochemistry, Geosystems*  
1181 (in review), 2019.

1182 Kissock, J.K., Finzel, E.S., Malone, D.H., and Craddock, J.P.: Lower–Middle Pennsylvanian strata  
1183 in the North American midcontinent record the interplay between erosional unroofing of the  
1184 Appalachians and eustatic sea-level rise: *Geosphere*, v. 14 (1), p. 141–161, 2018.

1185 Lawton, T.F., Buller, C.D., and Parr, T.R.: Provenance of a Permian erg on the western margin of  
1186 Pangea: Depositional system of the Kungurian (late Leonardian) Castle Valley and White Rim  
1187 sandstones and subjacent Cutler Group, Paradox Basin, Utah, USA: *Geosphere*, v. 11 (5), p. 1–  
1188 32, 2015.

1189 Lucas, S.G.: The Chinle Group: revised stratigraphy and biostratigraphy of Upper Triassic  
1190 nonmarine strata in the western United States, in: *Aspects of Mesozoic Geology and*  
1191 *Paleontology of the Colorado Plateau*, edited by: Morales, M., Museum of Northern Arizona  
1192 Bulletin 59, Flagstaff: Museum of Northern Arizona Press, p. 27–50., 1993.

1193 Ludwig, K.R.: Isoplot 3.6: Berkeley Geochronology Center Special Publication 4, 77 p., 2008.

1194 Marsh, A.D., Parker, W.G., Stockli, D.F., and Martz, J.W.: Regional correlation of the Sonsela  
1195 Member (Upper Triassic Chinle Formation) and detrital U-Pb zircon data from the Sonsela  
1196 Sandstone bed near the Sonsela Buttes, northeastern Arizona, USA, support the presence of a  
1197 distributive fluvial system: *Geosphere*, v. 15, <https://doi.org/10.1130/GES02004.1>, 2019.

1198 Martz, J.W. and Parker, W.G.: Revised lithostratigraphy of the Sonsela Member (Chinle  
1199 Formation, Upper Triassic) in the southwestern part of Petrified Forest National Park, Arizona:  
1200 PLoS ONE 5(2): e9329. doi:10.1371/journal.pone.0009329, 2010.

1201 Martz, J.W., Parker, W.G., Skinner, L., Raucchi, J.J., Umhoefer, P., and Blakey, R.C.: Geologic map  
1202 of Petrified Forest National Park, Arizona: Arizona Geological Survey Contributed Map CM-12-A,  
1203 1 map sheet, scale 1:50,000, 18 p., [http://repository.azgs.gov/uri\\_gin/azgs/dlio/1487](http://repository.azgs.gov/uri_gin/azgs/dlio/1487), 2012.

1204 Martz, J.W., Kirkland, J.I., Milner, A.R.C., Parker, W.G., Santucci, V.L.: Upper Triassic  
1205 lithostratigraphy, depositional systems, and vertebrate paleontology across southern Utah:  
1206 *Geology of the Intermountain West*, v. 4, p. 99-180, [https://www.utahgeology.org/wp-](https://www.utahgeology.org/wp-content/uploads/2018/05/GIW2017-v04-pp099-180-Martz.pdf)  
1207 [content/uploads/2018/05/GIW2017-v04-pp099-180-Martz.pdf](https://www.utahgeology.org/wp-content/uploads/2018/05/GIW2017-v04-pp099-180-Martz.pdf), 2017.

1208 Miller, J.S., Glazner, A.F., Walker, J.D., and Martin, M.W.: Geochronologic and isotopic evidence  
1209 for Triassic–Jurassic emplacement of the eugeoclinal allochthon in the Mojave Desert region,  
1210 California: *Geological Society of America Bulletin*, v. 107, p. 1441–1457, 1995.

1211 Nordt, L., Atchley, S., Dworkin, S.: Collapse of the Late Triassic megamonsoon in western  
1212 equatorial Pangea, present-day American southwest: *Geological Society of America Bulletin*, v.  
1213 127 (11/12), p. 1798–1815, 2015.

1214 Olsen, P. E., Kent, D.V., and Whiteside, H.: Implications of the Newark Supergroup-based  
1215 astrochronology and geomagnetic polarity time scale (Newark-APTS) for the tempo and mode  
1216 of the early diversification of the Dinosauria: *Earth and Environmental Science Transactions of*  
1217 *the Royal Society of Edinburgh*, v. 101, p. 201–229, 2011.

1218 Olsen, P., Geissman, J., Kent, D., Gehrels, G., and 23 others: Colorado Plateau Coring Project,  
1219 Phase I (CPCP-I): a continuously cored, globally exportable chronology of Triassic continental  
1220 environmental change from western North America: *Scientific Drilling*, v. 24, p. 15–40, 2018.

1221 Olsen, P.E., Laskar, J., Kent, D.V., Kinney, S.T., Reynolds, D.J., Sha, J. and Whiteside, J.H.:  
1222 Mapping Solar System chaos with the Geological Orrery: *Proceedings of the National Academy*  
1223 *of Sciences*, v. 116 (22), p. 10664-10673, 2019.

1224 Ortega-Flores, B., Solari, L., Lawton, T.F., and Ortega-Obregón, C.: Detrital-zircon record of  
1225 major Middle Triassic–Early Cretaceous provenance shift, central Mexico: demise of  
1226 Gondwanan continental fluvial systems and onset of backarc volcanism and sedimentation:  
1227 *International Geology Review*, v. 56 (2), p. 237-261, 2014.

1228 Paces, J.B., & Miller, J.D.: Precise U-Pb ages of Duluth Complex and related mafic intrusions,  
1229 northeastern Minnesota: Geochronological insights to physical, petrogenetic, paleomagnetic,  
1230 and tectonomagmatic processes associated with the 1.1 Ga midcontinent rift system: *Journal of*  
1231 *Geophysical Research*, v. 98 (B8), p. 13997–14013. <https://doi.org/10.1029/93JB01159>, 1993.

1232 Parker, W., and Martz, J.: Constraining the stratigraphic position of the Late Triassic (Norian)  
1233 Adamanian-Revueltian faunal transition in the Chinle Formation of Petrified Forest National  
1234 Park, Arizona: *Journal of Vertebrate Paleontology*, v. 29 (suppl. to 3), p. 162A, 2009.

1235 Parker, W.G., and Martz, J.W.: The Late Triassic (Norian) Adamanian–Revueltian tetrapod faunal  
1236 transition in the Chinle Formation of Petrified Forest National Park, Arizona, *Earth and*  
1237 *Environmental Science Transactions of the Royal Society of Edinburgh*: v. 101, p. 231–260,  
1238 2011.

1239 Pipiringos, G.N., O’Sullivan, R.B.: Principal unconformities in Triassic and Jurassic rocks, Western  
1240 Interior United States – a preliminary survey: *Geological Survey Professional Paper 1035-A*, 29  
1241 p., 1978.

1242 Pullen, A., Ibanez-Mejia, M., Gehrels, G., Giesler, D., and Pecha, M.: Optimization of a Laser  
1243 Ablation-Single Collector-Inductively Coupled Plasma-Mass Spectrometer (Thermo Element 2)  
1244 for Accurate, Precise, and Efficient Zircon U-Th-Pb Geochronology: *Geochemistry, Geophysics,*  
1245 *Geosystems*, v. 19. <https://doi.org/10.1029/2018GC007889>, 2018.

- 1246 Ramezani, J., Hoke, G.D., Fastovsky, D.E., Bowring, S.A., Therrien, F., Dworkin, S.I., Atchley, S.C.,  
1247 and Nordt, L.C.: High precision U-Pb zircon geochronology of the Late Triassic Chinle Formation,  
1248 Petrified Forest National Park (Arizona, USA): Temporal constraints on the early evolution of  
1249 dinosaurs: *Geological Society of America Bulletin*, v. 123, p. 2142–2159, 2011.
- 1250 Ramezani, J., Fastovsky, D.E., and Bowring, S.A.: Revised chronostratigraphy of the lower Chinle  
1251 Formation strata in Arizona Arizona and New Mexico (USA): high-precision U-Pb  
1252 geochronological constraints on the Late Triassic evolution of dinosaurs: *American Journal of  
1253 Science*, v. 314, p. 981–1008, 2014.
- 1254 Rasmussen, C., Mundil, R., Irmis, R.B., Geisler, D., Gehrels, G.E., Olsen, P.E., Kent, D.V., Lepre, C.,  
1255 Geissmann, J.W., and Parker, W.G.: A high-resolution age model for the Upper Triassic Chinle  
1256 Formation (Petrified Forest National Park, Arizona, USA) constrained by U-Pb geochronology  
1257 and magnetostratigraphy: implications for Late Triassic paleoecological and  
1258 paleoenvironmental change: *Geological Society of America Bulletin* (in review), 202019.
- 1259 Reichgelt, T., Parker, W.G., Martz, J.W., Conran, J.G., Cittert, J.H.A.K., Kürschner, W.M.: The  
1260 palynology of the Sonsela Member (Late Triassic, Norian) at Petrified Forest National Park,  
1261 Arizona, USA: *Review of Palaeobotany and Palynology*, v. 189, p. 18-28,  
1262 doi.org/10.1016/j.revpalbo.2012.11.001, 2013.
- 1263 Riggs, N.R., Lehman, T.M., Gehrels, G.E., and Dickinson, W.R.: Detrital zircon link between  
1264 headwaters and terminus of the Upper Triassic Chinle–Dockum paleoriver system: *Science*, v.  
1265 273, p. 97–100, 1996.
- 1266 Riggs, N.R., Ash, S.R., Barth, A.P., Gehrels, G.E., and Wooden, J.L.: Isotopic age of the Black  
1267 Forest Bed, Petrified Forest Member, Chinle Formation, Arizona: an example of dating a  
1268 continental sandstone: *Geological Society of America Bulletin*, v. 115, p. 1315–1323, 2003.
- 1269 Riggs, N.R., Barth, A.P., González-León, C., Jacobson, C.E., Howell, E., Wooden, J.E., and Walker,  
1270 J.D.: Provenance of Upper Triassic strata in southwestern North America as suggested by  
1271 isotopic analysis and chemistry of zircon crystals, in Rasbury, E.T., Hemming, S., and Riggs, N.,  
1272 eds., *Mineralogical and Geochemical Approaches to Provenance: Geological Society of America  
1273 Special Paper 487*, p. 13–36, doi: 10 .1130 /2012 .2487 (02), 2012.
- 1274 Riggs, N.R., Reynolds, S.J., Lindner, P.J., Howell, E.R., Barth, A.P., Parker, W.G., and Walker, J.D.:  
1275 The Early Mesozoic Cordilleran arc and Late Triassic paleotopography: The detrital record in  
1276 Upper Triassic sedimentary successions on and off the Colorado Plateau: *Geosphere*, v. 9, p.  
1277 602–613, 2013.
- 1278 Riggs, N.R., Oberling, Z.A., Howell, E.R., Parker, W.G., Barth, A.P., Cecil, M.R., and Martz, J.W.:  
1279 Sources of volcanic detritus in the basal Chinle Formation, southwestern Laurentia, and  
1280 implications for the Early Mesozoic magmatic arc: *Geosphere*, v. 12, p. 439–463, 2016.



1281 Saleeby, J., and Dunne, G.: Temporal and tectonic relations of early Mesozoic arc magmatism,  
1282 southern Sierra Nevada, California, in Anderson, T.H., Didenko, A.N., Johnson, C.L., Khanchuk,  
1283 A.I., and MacDonald, J.H., Jr., eds., Late Jurassic Margin of Laurasia—A Record of Faulting  
1284 Accommodating Plate Rotation: Geological Society of America Special Paper 513, p. 223–268,  
1285 2015.

1286 Saylor, J.E., and Sundell, K.E.: Quantifying comparison of large detrital geochronology data sets.  
1287 *Geosphere*12, 203–220, 2016.

1288 Saylor, J.E., Jordan, J.C., Sundell, K.E., Wang, X., Wang, S., and Deng, T.: Topographic growth of  
1289 the Jishi Shan and its impact on basin and hydrology evolution, NE Tibetan Plateau: *Basin*  
1290 *Research*, v. 30(3), p. 544-563, 2018.

1291 Stewart, J.H., Anderson, T.H., Haxel, G.B., Silver, L.T., and Wright, J.E.: Late Triassic  
1292 paleogeography of the southern Cordillera: The problem of a source for the voluminous  
1293 volcanic detritus in the Chinle Formation of the Colorado Plateau region: *Geology*, v. 14, p. 567–  
1294 570, 1986.

1295 Sundell, K.E., Saylor, J.E., and Pecha, M.: Sediment provenance and recycling of detrital zircons  
1296 from Cenozoic Altiplano strata in southern Peru and implications for the crustal evolution of  
1297 west-central South America: *Journal of South American Earth Sciences*, (in review), 2019.

1298 Surpless, K.D., Graham, S.A., Covault, J.A., and Wooden, J.L.: Does the Great Valley Group  
1299 contain Jurassic strata? Reevaluation of the age and early evolution of a classic forearc basin:  
1300 *Geology*, v. 34 (1), p. 21–24, 2006.

1301 Thomas, W.A., Gehrels, G.E., Greb, S.F., Nadon, G.C., Satkoski, A.M., and Romero, M.C.: Detrital  
1302 zircon grains and sediment dispersal in the Appalachian foreland: *Geosphere*, v. 13 (6), p. 2206-  
1303 2230, 2017.

1304 Thomas, W.A., Gehrels, G.E., Lawton, T., Satterfield, J., Romero, M., and Sundell, K.: Detrital  
1305 zircon grains and sediment dispersal from the Coahuila terrane of northern Mexico into the  
1306 Marathon foreland of the southern Midcontinent: *Geosphere*, v. 16 (in press), 2019.

1307 Tobisch, O.T., Fiske, R.S., Saleeby, J.B., Holt, E., and Sorensen, S.S.: Steep tilting of metavolcanic  
1308 rocks by multiple mechanisms, central Sierra Nevada, California: *Geological Society of America*  
1309 *Bulletin*, v. 112 (7), p. 1043–1058, 2000.

1310 Vermeesch, P.: Multi-sample comparison of detrital age distributions: *Chemical Geology*, v. 341,  
1311 p. 140-146, 2013.

1312 [Vermeesch, P.: Dissimilarity measures in detrital geochronology: \*Earth-Science Reviews\*, v. 178:](#)  
1313 [p. 310–321, 2018a. doi: 10.1016/j.earscirev.2017.11.027.](#)

1314 [Vermeesch, P.: Statistics for fission tracks. In Malus´a, M. and Fitzgerald, P., editors, \*Fission\*](#)

1315 [track thermochronology and its application to geology. Springer, 2018b.](#)

1316 [Vermeesch, P.: Maximum depositional age estimation revisited: Geoscience Frontiers, in](#)  
1317 [review.](#)

1318 Wissink, G.K., Wilkinson, B.H., and Hoke, G.D.: Pairwise sample comparisons and  
1319 multidimensional scaling of detrital zircon ages with examples from the North American  
1320 platform, basin, and passive margin settings: *Lithosphere*, <https://doi.org/10.1130/L700.1>,  
1321 2018.

1322 Woody, D.T.: Revised stratigraphy of the lower Chinle Formation (Upper Triassic) of Petrified  
1323 Forest National Park, Arizona: *Museum of Northern Arizona Bulletin*, v. 62, p. 17–45, 2006.

1324 Wright, J.E., and Wyld, S.J.: Alternative tectonic model for Late Jurassic through Early  
1325 Cretaceous evolution of the Great Valley Group, California, in Cloos, M., Carlson, W.D., Gilbert,  
1326 M.C., Liou, J.G., and Sorensen, S.S., eds., *Convergent Margin Terranes and Associated Regions:*  
1327 *A Tribute to W.G. Ernst: Geological Society of America Special Paper 419*, p. 1-15, 2007.

1328 Xie, X., Anthony, J.M., and Busbey, A.B.: Provenance of Permian Delaware Mountain Group,  
1329 central and southern Delaware basin, and implications of sediment dispersal pathway near the  
1330 southwestern terminus of Pangea: *International Geology Review*, DOI:  
1331 10.1080/00206814.2018.1425925, 2018.

1332 **FIGURE CAPTIONS**

1333 **Figure 1.** Map showing the main basement provinces of southern North America and Mexico.  
1334 Also shown are locations of the study area within the Colorado Plateau, outlines of Ancestral  
1335 Rocky Mountains uplifts, and the Permian-Triassic magmatic arc along the continental margin  
1336 of southwestern North America. Modified from Gehrels et al. (2011).

1337 **Figure 2.** Strata encountered in the Colorado Plateau Coring Project (adapted from Olsen et al.,  
1338 2018). Sampled horizons are shown relative to core depth, stratigraphic depth, and  
1339 stratigraphic nomenclature relevant for the Petrified Forest region. Detailed descriptions of  
1340 samples are provided in DR Table 1; images of the sampled material are presented in Appendix  
1341 1.

1342 **Figure 3.** Normalized probability density plots of U-Pb (zircon) ages from source terranes.  
1343 Distinctive age groups include 1750-1620 Ma and 1520-1360 Ma ages from southwest Laurentia  
1344 basement provinces, 1240-960 Ma ages from Grenville-age provinces exposed in the  
1345 Appalachian and Ouachita orogens, 640-570 Ma and 480-370 Ma ages characteristic of the  
1346 Appalachian orogen, 670-300 Ma ages from the Ouachita orogen, 300-260 Ma ages from the  
1347 East Mexico arc, and 260-200 Ma ages belonging to the Cordilleran magmatic arc of  
1348 southwestern North America. See text for sources of information.

1349 **Figure 4.** Plot showing the accuracy of  $^{206}\text{Pb}^*/^{238}\text{U}$  dates of secondary standards analyzed  
1350 during the current study. Each pair of symbols represents the weighted mean age and  $2\sigma$   
1351 uncertainty of R33 and FC-1 analyses conducted with each sample, expressed as % offset from  
1352 reported ID-TIMS dates of 1099.9 Ma for FC-1 (Paces and Miller, 1993) and 419.26 Ma for R33  
1353 (Black et al., 2004). For FC-1, 1065 analyses are reported, with MSWD = 0.95 for all analyses. For  
1354 R33, 295 analyses are reported, with MSWD = 0.92 for all analyses. Data are reported in DR  
1355 Table 7.

1356 **Figure 5.** Normalized probability density plots of detrital zircon ages from our sample of the  
1357 Coconino Sandstone and from other lower Permian sandstones of the Colorado Plateau.  
1358 Numbers of constituent analyses are shown for each sample. Data are from <sup>1</sup>Dickinson and  
1359 Gehrels (2003), <sup>2</sup>Gehrels et al. (2011), <sup>3</sup>Lawton et al. (2015), and <sup>4</sup>this study. Shown for  
1360 reference are age ranges from the Appalachian orogen (purple bands) and from local basement  
1361 rocks (blue bands) (from Figure 3), which are interpreted by previous researchers to have  
1362 sourced most of the detritus in these units. Also shown is our sample 383-2, which is  
1363 interpreted to belong to the Wupatki Member of the Moenkopi Formation, but has an age  
1364 signature characteristic of lower Permian strata of the Colorado Plateau.

1365 **Figure 6.** Probability density plots of detrital zircon ages from four samples from the Moenkopi  
1366 Formation (lower four curves) as well as a Moenkopi sample from Dickinson and Gehrels  
1367 (2008). Numbers of constituent analyses are shown for each sample. Samples 349-3, 335-1,  
1368 327-2, and 319-2, plus the sample from Dickinson and Gehrels (2008), are all from the Holbrook

1369 Member. Sample 383-2 is interpreted to belong to the Wupatki Member, but has an age  
1370 distribution that resembles lower Permian strata. Source regions are interpreted to include  
1371 local basement rocks (blue bands), the Ouachita orogen (green bands), the East Mexico arc (red  
1372 band), and the Late Permian-Triassic arc built along the Cordilleran margin (orange band).

1373 **Figure 7.** Normalized probability density plots of detrital zircon ages from twenty-four samples  
1374 from the Mesa Redondo, Blue Mesa, Sonsela, and Petrified Forest Members of the Chinle  
1375 Formation. Numbers of constituent analyses are shown for each sample. Age distributions older  
1376 than 240 Ma are exaggerated by 10x. Black tick marks indicate the interpreted maximum  
1377 depositional ages for each sample (from DR Table 6). Source regions are interpreted to include  
1378 local basement rocks (blue bands), the Ouachita orogen (green bands), the East Mexico arc (red  
1379 band), and the Late Permian-Triassic arc built along the Cordilleran margin (orange band).  
1380 Percent of all grains that are <240 Ma in age are shown for each sample on the left.

1381 **Figure 8.** Normalized probability density plots of detrital zircon ages from each set of samples  
1382 analyzed in this study. Numbers of constituent analyses are shown for each sample. Age  
1383 distributions older than 240 Ma for Chinle strata are exaggerated by 10x relative to <240 Ma  
1384 ages. Age distributions for Moenkopi and Coconino Sandstones are exaggerated by 5x relative  
1385 to Chinle ages. Source regions are interpreted to include local basement rocks (blue bands), the  
1386 Ouachita orogen (green bands), the East Mexico arc (red band), and the Late Permian-Triassic  
1387 arc built along the Cordilleran margin (orange band). Results from sample 383-2 are not  
1388 included in this plot because of its uncertain stratigraphic position. Data from sample 131-2 are  
1389 omitted because they differ from ages present in other samples from the Petrified Forest  
1390 Member. Percent of all grains that are <240 Ma in age are shown for each sample on the left.

1391 **Figure 9.** MDS plot ([Vermeesch, 2013](#)) comparing age distributions of samples analyzed herein  
1392 with each other and with possible source areas. MDS (metric) analyses ~~are based on the KS-D~~  
1393 ~~values calculated from kernel density estimates of the age distributions~~~~cross-correlation~~  
1394 ~~coefficient, and~~ were conducted using the software of Saylor et al. (2018). Data from samples  
1395 analyzed herein are in DR Table 3. Ages for source regions are from the sources cited in the  
1396 text. ~~Stars represent MDS values for sets of examples. Samples 383-2 with the exception that~~  
1397 ~~sample 131 is not included with other Petrified Forest samples. Stars represent MDS values for~~  
1398 ~~sets of examples, with the exception that sample 131-2 is not included with other Petrified~~  
1399 ~~Forest samples.~~

1400 **Figure 10.** Density distributions of U concentration versus U/Th for Triassic grains in the four  
1401 chronostratigraphic units recognized in this study. Plots made with Hf density plotter software  
1402 of Sundell et al. (2019).

1403 **Figure 11.** MDS plot comparing age distributions of Permian strata of the Colorado Plateau with  
1404 each other and with potential source regions including the Appalachian orogen, Ouachita  
1405 orogen, and basement rocks of southwestern North America. Data sources are described in  
1406 Figures 3 and 4. The data support the interpretation of Lawton et al. (2015) that the Coconino,

1407 Cedar Mesa, and White Rim sandstones (cool shades) belong to a regional blanket of eolian  
1408 strata that was derived largely from the Appalachian and/or Ouachita orogen, where strata of  
1409 the Castle Valley and Cutler formations (warm shades) include greater proportions of detritus  
1410 derived from local basement sources.

1411 **Figure 12.** Sketch map of relevant tectonic features in southwestern Laurentia during Late  
1412 Triassic time [adapted from Figure 42 of Dickinson (2018)].

1413 **Figure 13.** Plot showing the available chronologic information for strata of the Chinle Formation  
1414 from the study area. LA-ICPMS results are shown using red crosses for interpreted maximum  
1415 depositional ages [using the minimum age approach of Vermeesch (2020)], and various symbols  
1416 for the four age estimates (and the average) of the youngest cluster. Red arrows indicate that  
1417 LA-ICPMS ages may be compromised by Pb loss (DR Table 6). ~~interpreted maximum~~  
1418 ~~depositional ages (and 2 $\sigma$  uncertainties) for each sample, as determined by the four methods~~  
1419 ~~described above and reported in DR Table 6. Preferred ages (vertical red lines) are the average~~  
1420 ~~of the ages calculated by these four methods.~~ CA-TIMS and ID-TIMS ages are shown in  
1421 approximate stratigraphic position (as shown by Kent et al., 2019), with outcrop samples in gray  
1422 symbols and core samples using black symbols. Smaller symbols represent ID-TIMS ages or CA-  
1423 TIMS ages based on a single age or of uncertain reliability. Stratigraphic units are keyed to  
1424 dominant rock type, with brown = mudstone and siltstone, yellow = sandstone, pink =  
1425 bentonite. Average grain size of each sample is shown with bars on left (from Appendix 1 and  
1426 DR Table 1). PDP curves to right show 2.0 Ga to 240 Ma ages, as plotted on Figure 7. Also shown  
1427 are age models of Kent et al. (2019) and Rasmussen et al. (202019). Vertical red bands show  
1428 interpreted ages of main clusters of LA-ICPMS maximum depositional ages.

1429 Curves across top of diagram show the distribution of ages from (1) fore-arc strata of the  
1430 Barranca and El Antimonio Groups in Sonora (Gonzalez-Leon et al., 2009; Gehrels and Pecha,  
1431 2014) and the Great Valley Group in California (DeGraaff-Surpless et al., 2002; Surpless et al.,  
1432 2006; Wright and Wyld, 2007), (2) Permian-Triassic igneous rocks in California (Chen and  
1433 Moore, 2982; Miller et al., 1995; Tobisch et al., 2000; Barth and Wooden, 2006, 2011, 2013;  
1434 Saleeby and Dunne, 2015), and (3) strata of the Chinle Formation in other parts of the Colorado  
1435 Plateau (Dickinson and Gehrels, 2008; Riggs et al., 2012; Marsh et al., 2019). Diamond-shaped  
1436 symbols beneath curves represent individual ages.

1437 **Figure 14.** Depositional model of strata of the Chinle Formation encountered in the CPCP core.  
1438 Each time slice contains information about the dominant grain size of the host sedimentary  
1439 rock, the abundance of syn-depositional-age zircon grains that are interpreted to be air-fall in  
1440 origin, and the abundance of recycled zircon grains that pre-date deposition.